



**Lehrstuhl für  
Technische Dynamik**  
Prof. Dr.-Ing. habil. Sigrid Leyendecker

# Report

## Chair of Applied Dynamics

### January 2013 – December 2013



**FRIEDRICH-ALEXANDER  
UNIVERSITÄT  
ERLANGEN-NÜRNBERG**  
TECHNISCHE FAKULTÄT

© 2013

Prof. Dr.-Ing. habil. S. Leyendecker

Lehrstuhl für Technische Dynamik

Universität Erlangen-Nürnberg

Haberstrasse 1

91058 Erlangen

Tel.: 09131 8561000

Fax.: 09131 8561011

www: <http://www.ltd.tf.uni-erlangen.de>

Editor: N. Kondratieva

All rights reserved. Without explicit permission of the authors it is not allowed to copy this publication or parts of it, neither by photocopy nor in electronic media.

# Contents

<b>1</b>	<b>Preface</b>	<b>4</b>
<b>2</b>	<b>Team</b>	<b>5</b>
<b>3</b>	<b>Research</b>	<b>7</b>
3.1	Emmy Noether Independent Junior Research Group . . . . .	7
3.2	Bionicum . . . . .	7
3.3	Cooperation partners . . . . .	7
3.4	Scientific reports . . . . .	7
<b>4</b>	<b>Activities</b>	<b>31</b>
4.1	Teaching . . . . .	31
4.2	Seminar for Mechanics . . . . .	32
4.3	Dynamics laboratory . . . . .	34
4.4	Summer schools . . . . .	35
<b>5</b>	<b>Publications</b>	<b>36</b>
5.1	Book chapters . . . . .	36
5.2	Reviewed journal publications . . . . .	36
5.3	Reviewed proceeding publications . . . . .	36
5.4	Talks . . . . .	37
<b>6</b>	<b>Social events</b>	<b>39</b>

## 1 Preface

This report summarises the activities in research and teaching of the Chair of Applied Dynamics at the University of Erlangen-Nuremberg between January 2013 and December 2013.

Part of LTD is the Independent Junior Research Group in the DFG Emmy Noether Programme ‘Simulation and optimal control of the dynamics of multibody systems in biomechanics and robotics’ that has been at the University of Kaiserslautern from May 2009 to March 2011. Research topics are situated in the field of computational mechanics, in particular dynamics and applied mathematics with focus on the simulation of human motion (everyday movements and sports) and robot dynamics as well as the optimization and optimal control of their dynamics.



## 2 Team

### chair holder

Prof. Dr.-Ing. habil. Sigrid Leyendecker

### technical staff

Beate Hegen

Dipl.-Ing. (FH) Natalia Kondratieva

Sven Lässig

### academic scientist

Dr. rer. nat. Holger Lang

### postdoc

Dr. Odysseas T. Kosmas

### scientific staff

Dipl.-Ing. Nathanael Bach

since 01.10.2013

Dipl.-Ing. Tobias Gail

Dipl.-Ing. Michael W. Koch

Dipl.-Ing. Thomas Leitz

Dipl.-Ing. Ramona Maas

until 31.07.2013

Dipl.-Math. Maik Ringkamp

Dipl.-Ing. Tristan Schlögl

since 01.03.2013

### students

Theresa Ach

Lukas Allabar

Tobias Bader

Andreas Enzenhöfer

Lukas Erdt

Markus Labus

Hannah Laube

Antonia Lion

Rene Rathman

Manuel Roppelt

Sebastian Riedel

Sebastian Scheiterer

Simon Schindler

Selina Scherzer

Johannes Vorndran

Sabine Weingärtner

Theresa Wenger

Johannes Zapf

Fabian Zimmer

Daniel Zint

Natalie Zipf



B. Hegen



N. Kondratieva



S. Lässig



H. Lang



O.T. Kosmas



N. Bach



T. Gail



M.W. Koch



T. Leitz



R. Maas



M. Ringkamp



T. Schlögl



S. Leyendecker

## 3 Research

### 3.1 Emmy Noether Independent Junior Research Group

The Emmy Noether Programme by the German Research Foundation (DFG) supports young researchers in achieving independence at an early stage of their scientific careers. Between May 2009 and March 2011, the Emmy Noether Independent Junior Research Group ‘Simulation and optimal control of the dynamics of multibody systems in biomechanics and robotics’ has been affiliated with the University of Kaiserslautern. The group has been transferred to the University of Erlangen-Nuremberg in April 2011 being now part of the Chair of Applied Dynamics.

### 3.2 Bionicum

The Bavarian Environment Agency (LfU) (being the central authority for environmental protection and nature conservation, geology and water resources management) has established the centre for bionics ‘bionicum’ in 2012, consisting of a visitors centre in the Tiergarten of the City of Nuremberg with a permanent exhibition and three research projects with a total financial volume of eight million Euro. One of the projects investigates artificial muscles. The modeling and simulation of the dielectric elastomer actors is developed at the LTD while the Institute for Factory Automation and Production Systems (FAPS) works on the fabrication.

### 3.3 Cooperation partners

Besides numerous worldwide cooperations with scientists in academia, the LTD is in contact with other institutions and industrial partners. The LTD cooperates with the Fraunhofer Institute for Industrial and Economical Mathematics (ITWM) in Kaiserslautern on common interests like biomechanics and nonlinear rod dynamics for wind turbine rotor blades.

### 3.4 Scientific reports

The following pages present a short overview on ongoing research projects pursued at the Chair of Applied Dynamics. These are partly financed by third-party funding (German Research Foundation (DFG), Bavarian Environment Agency (LfU)) and in addition by the core support of the university.

#### Research topics

*Numerical experiments for viscoelastic Cosserat rods with Kelvin-Voigt damping*  
Holger Lang, Sigrid Leyendecker, Joachim Linn

*On frequency estimations in phase fitted variational integrators for the general N-body problem*  
Odysseas T. Kosmas, Sigrid Leyendecker

*Computing time investigations of variational multirate systems*  
Tobias Gail, Sigrid Leyendecker

*Optimal control of standing high and long jumps*  
Michael W. Koch, Sigrid Leyendecker

*Lie group variational integrators with quaternion parametrization of rotations*  
Thomas Leitz, Sigrid Leyendecker

*On optimal control simulations of throwing*  
 Ramona Maas, Sigrid Leyendecker

*Identifying various types of Pareto sets in multiobjective optimal control of multibody dynamics*  
 Maik Ringkamp, Sigrid Leyendecker, Sina Ober-Blöbaum

*Finite element modelling of dielectric elastomers*  
 Tristan Schlögl, Sigrid Leyendecker

## Numerical experiments for viscoelastic Cosserat rods with Kelvin-Voigt damping

Holger Lang, Sigrid Leyendecker, Joachim Linn

Geometrically exact rod models of Cosserat type [5] still provide an interesting topic of research in computational mechanics. In realistic applications, simulation models for computing the transient response of structural members to dynamic excitations have to account for dissipative effects. In particular, in the case of geometrically exact rods, any approach to model viscous damping requires the inclusion of a frame-indifferent viscoelastic constitutive model already on the level of the continuum formulation of the structural model, such that large displacements and finite rotations can be handled properly.

The configuration of a Cosserat rod is uniquely defined by its centerline  $\varphi(s, t) \in \mathbb{R}^3$  of mass centroids and its orthonormal, right-handed frame field  $\mathbf{R}(s, t) \in SO(3)$ . Always,  $0 \leq s \leq L$  denotes the *arclength* parameter,  $t$  denotes the *time*. We write  $' = \partial_s$  and  $\dot{\phantom{x}} = \partial_t$  for the corresponding partial derivatives. For the sake of simplicity, we assume that the rod is straight in its undeformed reference configuration. Then, the *material strain vector* is defined by  $\mathbf{\Gamma} = \mathbf{R}^\top \partial_s \varphi - \mathbf{e}_3$ . The *material curvature vector*  $\mathbf{K} \in \mathbb{R}^3$  is defined as the unique axial vector corresponding to the skew symmetric tensor  $\mathbf{R}^\top \partial_s \mathbf{R} \in so(3)$ .

In [2], we formulate a *Kelvin-Voigt* type constitutive model by adding viscous contributions to the material stress resultants (forces)  $\mathbf{F}$  and stress couples (momenta)  $\mathbf{M}$ . These are assumed to be proportional to the *rates*  $\dot{\mathbf{\Gamma}}$  and  $\dot{\mathbf{K}}$  of the material strain and curvature measures of the rod. In the *effective material constitutive equations*

$$\mathbf{F} = \mathbb{C}_\Gamma \mathbf{\Gamma} + \mathbb{V}_\Gamma \dot{\mathbf{\Gamma}} \quad \text{and} \quad \mathbf{M} = \mathbb{C}_K \mathbf{K} + \mathbb{V}_K \dot{\mathbf{K}}, \quad (1)$$

where  $\mathbb{C}_\Gamma = \text{diag}(GA, GA, EA)$ ,  $\mathbb{C}_K = \text{diag}(EI_1, EI_2, GJ)$ ,  $\mathbb{V}_\Gamma = \text{diag}(\eta_G A, \eta_G A, \eta_E A)$ ,  $\mathbb{V}_K = \text{diag}(\eta_E I_1, \eta_E I_2, \eta_G J)$ , the elastic properties of the rod are determined by the *effective stiffness parameters*  $GA$ ,  $EA$ ,  $EI_1$ ,  $EI_2$  and  $GJ$  in terms of the geometric data  $A$ ,  $I_1$ ,  $I_2$  and  $J$  and the *extensional (Young's) modulus*  $E$  and *shear modulus*  $G$ .  $A$  denotes the *area* of the cross section,  $I_1$  and  $I_2$  denote its *geometric momenta of inertia*.  $J = I_1 + I_2$  is the polar moment of inertia.

In contribution [3], we present a derivation of the Kelvin-Voigt rod model from three-dimensional continuum theory. In addition to these effective stiffness parameters, we derive explicit formulas for the damping parameters of the model given by the *effective viscous parameters*  $\eta_G A$ ,  $\eta_E A$ ,  $\eta_E I_1$ ,  $\eta_E I_2$  and  $\eta_G J$ , again in terms of the geometry data and the *extensional* and *shear viscosity*  $\eta_E$  and  $\eta_G$ . These damping parameters model the integrated cross-sectional viscous damping behaviour associated to the basic deformation modes (extension, transverse shearing, bending and torsion) in the same way as the well known stiffness parameters model the corresponding elastic response. Further, it is derived from three-dimensional elasticity theory that for a linear, isotropic and homogeneous viscoelastic material

with Kelvin-Voigt damping, the internal forces resp. momenta are related to the strain resp. curvature according to (1).

With the *spatial force*  $\mathbf{f} = \mathbf{R}\mathbf{F}$  and *spatial moment*  $\mathbf{m} = \mathbf{R}\mathbf{M}$ , the dynamic balance equations take the well-known form

$$\begin{cases} \rho A \ddot{\varphi} &= \partial_s \mathbf{f} \\ \rho \mathbf{I} \dot{\boldsymbol{\omega}} &= \partial_s \mathbf{m} + \partial_s \varphi \times \mathbf{f} - \rho \boldsymbol{\omega} \times \mathbf{I} \boldsymbol{\omega} \end{cases}, \quad (2)$$

where  $\mathbf{I}(s, t)$  is the geometric moment of inertia tensor,  $\boldsymbol{\omega}(s, t)$  is the spatial angular velocity and  $\rho$  denotes the density [5].

In [4], we present first results of such a systematic investigation obtained from viscous and dynamic simulations. Here, we study the influence of the viscosity  $\eta_E$  on *extensional vibrations* as an example. In practical applications, extensional oscillations usually are of subordinate importance. Therefore, we are looking for some ‘critical’ value  $\eta_{E,cr}$  that separates oscillatory from purely viscous behaviour. In linear structural dynamics, the concept of *modal damping* is well-established [1]. The aim is to mimic this concept and to transfer it to the nonlinear regime. The idea is to linearise the equations of motion (2) for an undeformed, straight rod and then to perform complex modal analysis. Linearisation yields

$$\rho A \ddot{u} = \partial_s (EA u' + \eta_E A \dot{u}'), \quad (3)$$

where  $u$  is the (small) extensional displacement. For  $\eta_E = 0$ , the extensional beam (3), is thoroughly discussed in [1]. If we assume that the material and geometry data are constant along the rod, (3) becomes

$$\rho \ddot{u} = E u'' + \eta_E \dot{u}''.$$

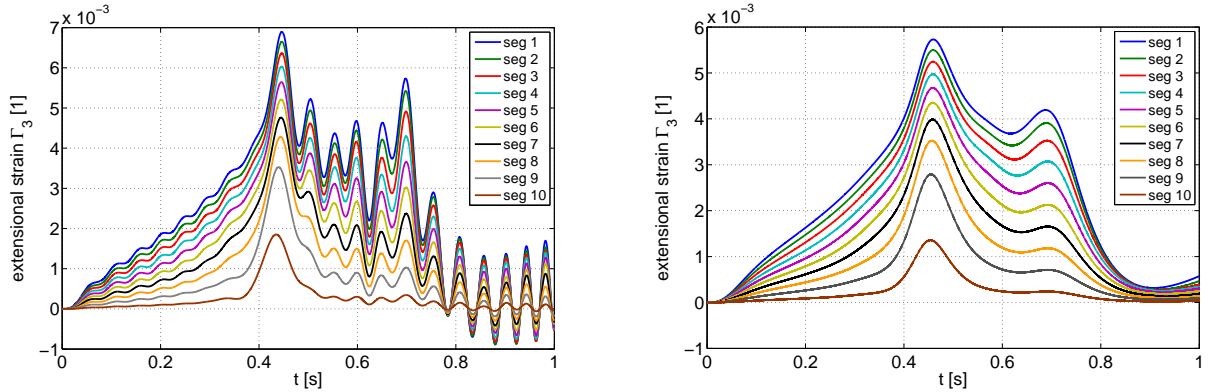


Figure 1: Extensional strains during a typical nonlinear dynamic motion. The undamped, first axial eigenfrequency  $\omega_0 = 105.9 \text{ rad s}^{-1} \simeq 16.9 \text{ Hz}$  (left) is critically damped out (right).

With the ansatz  $u(s, t) = U(s)e^{\lambda t}$  with a complex frequency  $\lambda$  and an unknown complex valued mode shape function  $U(s)$ , we obtain  $U''(s) = \mu^2 U(s)$ , where  $\mu^2(E + \eta_E \lambda) = \rho \lambda^2$ . The general solution of this differential equation is given by  $U(s) = C_+ e^{\mu s} + C_- e^{-\mu s}$ . For boundary conditions, where  $u(0) = 0$  and  $u'(L) = 0$ , it follows that  $C_+ = -C_-$ . Therefore,  $\cosh(\mu L) = 0$  and  $\mu = \mu_n = \frac{(2n+1)\pi}{2L} i$  with an integer  $n$ . Solving the remaining quadratic equation for  $\lambda$ , we obtain the complex eigenfrequency  $\lambda = \lambda_{n,\pm} = \frac{1}{2\rho} (\eta_E \mu_n^2 \pm \mu_n (\eta_E^2 \mu_n^2 + 4E\rho)^{1/2})$  for each such  $n$ . Now, the  $n$ -th mode is critically damped, if the  $n$ -th radicand vanishes. Therefore, any choice  $\eta_E$  larger than the *critical extensional viscosity*

$$\eta_{E,cr} = \frac{4L}{\pi} \sqrt{E\rho} \quad (4)$$

should damp out *all* oscillations resulting from extensional excitement. This is in fact the case, as the following example demonstrates.

A rod, made of rubber-like material, is subjected to its own gravitational force so that it performs (large) nonlinear bending and (small) extensional oscillations. The parameters are chosen as  $E = 5.00 \cdot 10^6 \text{ N m}^{-2}$ ,  $A = 7.85 \cdot 10^{-5} \text{ m}^2$ ,  $G = 1.67 \cdot 10^6 \text{ N m}^{-2}$ ,  $I_1 = I_2 = 4.91 \cdot 10^{-10} \text{ m}^4$  and  $\varrho = 1.10 \cdot 10^3 \text{ kg m}^{-3}$ . Figure 1 shows the extensional strain  $\langle \mathbf{\Gamma}, \mathbf{e}_3 \rangle$  for each of the rod segments as a function of time. The oscillations of the ‘first extensional eigenfrequency’ are clearly visible in the left picture, where  $\eta_E = 0$ . For the choice  $\eta_E = \eta_{E,\text{cr}} = 9.44 \cdot 10^5 \text{ N m}^{-2} \text{ s}$  according to (4) precisely these oscillations are damped out, as can be seen in the right plot in Figure 1. The remaining transients – their frequency is much smaller – result from the gross overall bending of the rod.

For the numerical example in this article, we use a spatial discretisation scheme on a staggered grid, proposed in [2]. More numerical examples can be found in [4].

## References

- [1] R.R. Craig, and A.J. Kurdila. *Fundamentals of Structural Dynamics*. John Wiley & Sons, 2006.
- [2] H. Lang, J. Linn, and M. Arnold. *Multibody dynamics simulation of geometrically exact Cosserat rods*. *Multibody System Dynamics*, Vol. 25(3), pp. 285-312, 2011.
- [3] J. Linn, H. Lang, and A. Tuganov. *Geometrically exact Cosserat rods with Kelvin-Voigt type viscous damping*. *Mech. Sci.*, Vol. 4, pp. 79-96, 2013.
- [4] H. Lang, S. Leyendecker, and J. Linn. *Numerical experiments for viscoelastic Cosserat rods with Kelvin-Voigt damping*. *Proceedings of the ECCOMAS Thematic Conference on Multibody Dynamics*, Zagreb, Croatia, 1-4 July, 2013.
- [5] J.C. Simo. *A finite strain beam formulation: the three dimensional dynamic problem – Part I*. *Comp. Meth. Appl. Mech. Engrg.*, Vol. 49, pp. 55-70, 1985.

## On frequency estimations in phase fitted variational integrators for the general N-body problem

Odysseas Kosmas, Sigrid Leyendecker

One of the most difficult problems in the numerical solution of ordinary differential equations is the development of methods for simulating highly oscillatory systems. Standard numerical schemes can require a huge number of time steps to track the oscillations, and even with small step sizes they can alter the dynamics, unless the method is chosen carefully. For that, it is useful to introduce geometric integrators, that is, numerical schemes which preserve some features of geometric nature of the dynamical systems. Usually, these integrators can run in simulations for long time with lower spurious effects (for instance, better energy behavior for conservative systems) than the traditional ones [1, 2].

For the derivation of high order variational integrators, we need to recall discrete variational calculus, see [1] and references therein. A discrete Lagrangian is a map  $L_d : Q \times Q \rightarrow \mathbb{R}$  defined on two copies of the configuration manifold  $Q$ , which may be considered as an approximation of a continuous action with Lagrangian  $L : TQ \rightarrow \mathbb{R}$ , i.e.  $L_d(q_k, q_{k+1}) \approx \int_{t_k}^{t_{k+1}} L(q, \dot{q}) dt$  in the time interval  $[t_k, t_{k+1}] \subset \mathbb{R}$ . The action sum  $S_d : Q^{N+1} \rightarrow \mathbb{R}$ ,  $N \in \mathbb{N}$  corresponding to the Lagrangian  $L_d$  is defined as  $S_d(\gamma_d) = \sum_{k=0}^{N-1} L_d(q_k, q_{k+1})$  with  $\gamma_d = (q_0, \dots, q_N)$  representing the discrete trajectory. The discrete Hamilton’s principle states that a motion  $\gamma_d$  of the discrete mechanical system extremizes the action

sum, i.e.  $\delta S_d = 0$ . By differentiation and rearrangement of the terms and having in mind that both  $q_0$  and  $q_N$  are fixed, the discrete Euler-Lagrange equations (DEL) are obtained [1]

$$D_2 L_d(q_{k-1}, q_k) + D_1 L_d(q_k, q_{k+1}) = 0, \quad k = 1, \dots, N-1 \quad (1)$$

where the notation  $D_i L_d$  indicates the slot derivative with respect to the  $i$ -th argument of  $L_d$ .

### Discrete Lagrangian using interpolation techniques

To construct high order methods, we approximate the action integral along the curve segment between  $q_k$  and  $q_{k+1}$  using a discrete Lagrangian that depends only on the end points. We obtain expressions for configurations  $q_k^j$  and velocities  $\dot{q}_k^j$  for  $j = 0, \dots, S-1$ ,  $S \in \mathbb{N}$  at time  $t_k^j \in [t_k, t_{k+1}]$  by expressing  $t_k^j = t_k + C_k^j h$  for  $C_k^j \in [0, 1]$  such that  $C_k^0 = 0, C_k^{S-1} = 1$  using

$$q_k^j = g_1(t_k^j)q_k + g_2(t_k^j)q_{k+1}, \quad \dot{q}_k^j = \dot{g}_1(t_k^j)q_k + \dot{g}_2(t_k^j)q_{k+1} \quad (2)$$

where  $h \in \mathbb{R}$  is the time step. We choose functions

$$g_1(t_k^j) = \sin\left(u - \frac{t_k^j - t_k}{h}u\right) (\sin u)^{-1}, \quad g_2(t_k^j) = \sin\left(\frac{t_k^j - t_k}{h}u\right) (\sin u)^{-1} \quad (3)$$

to represent the oscillatory behavior of the solution, see [3, 4]. For continuity,  $g_1(t_{k+1}) = g_2(t_k) = 0$  and  $g_1(t_k) = g_2(t_{k+1}) = 1$  is required.

For any choice of interpolation in (2), we define the discrete Lagrangian by the weighted sum  $L_d(q_k, q_{k+1}) = h \sum_{j=0}^{S-1} w^j L(q(t_k^j), \dot{q}(t_k^j))$ , where it can be easily proved that for maximal algebraic order,  $\sum_{j=0}^{S-1} w^j (C_k^j)^m = \frac{1}{m+1}$  where  $m = 0, 1, \dots, S-1$  and  $k = 0, 1, \dots, N-1$  must hold, see [3, 4].

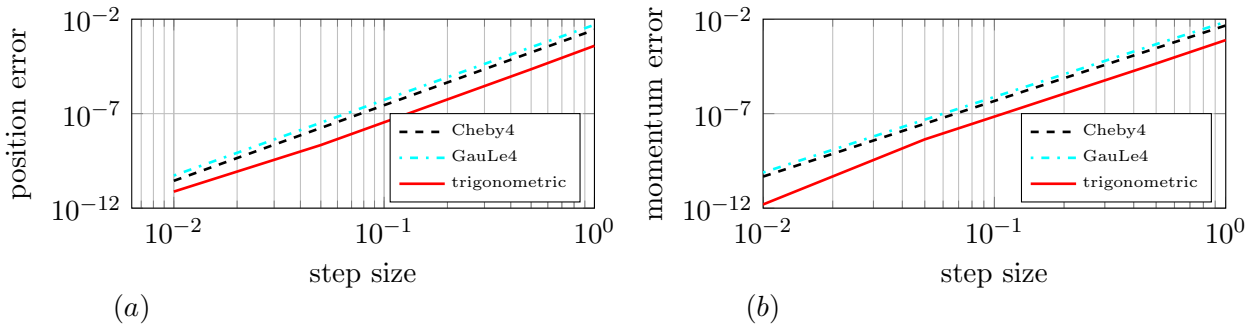


Figure 1: Harmonic oscillator with  $\omega = 1$  and  $S = 5$ . Global errors for (a) the position and (b) the momentum using five step sizes  $h$  for the GauLe4, Cheby4 [6] and the trigonometric interpolation method.

For the case of the harmonic oscillator with frequency  $\omega$ , the Lagrangian function is  $L = \dot{q}^2/2 - \omega^2 q^2/2$ , which leads to discrete Euler-Lagrange equations (1)

$$q_{k+1} + \frac{\sum_{j=0}^{S-1} w^j \left[ \dot{g}_1(t_k^j)^2 + \dot{g}_2(t_k^j)^2 - \omega^2 (g_1(t_k^j)^2 + g_2(t_k^j)^2) \right]}{\sum_{j=0}^{S-1} w^j \left[ \dot{g}_1(t_k^j) \dot{g}_2(t_k^j) - \omega^2 g_1(t_k^j) g_2(t_k^j) \right]} q_k + q_{k-1} = 0. \quad (4)$$

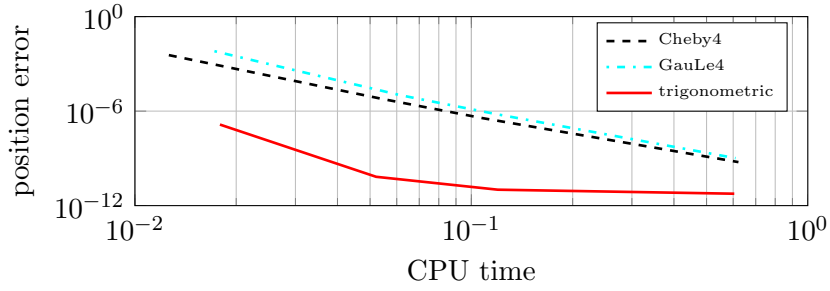


Figure 2: Harmonic oscillator with  $\omega = 1$ . CPU time versus position error (absolute value) for method using trigonometric interpolation for  $S = 5$  and for the GauLe4, Cheby4 [6].

To test the numerical convergence of the proposed method, we choose the initial conditions  $(q_0, p_0) = (2, 2)$  and the time interval  $[0, 3]$  as in [6]. The global errors for the position and momentum components at  $t = 3$  for time steps  $h \in \{0.01, 0.05, 0.1, 0.5, 1\}$  are compared to those of [6], i.e. Cheby4 and GauLe4 for the case of the harmonic oscillator with  $\omega = 1$ , see Figure 1. While all methods are of the same order four, for all the step sizes that are tested, the smallest errors in position and momentum are obtained with the phase fitted method derived using trigonometric interpolation, i.e. for  $u = \omega h$ , see also Figure 2.

### Frequency estimation for mass points motion in three dimensions

Applying the interpolation technique with the above trigonometric expressions, the parameter  $u$  can be chosen as  $u = \omega h$  [3, 4]. For problems that include a constant and known domain frequency  $\omega$  (such as the harmonic oscillator) the parameter  $u$  can be easily computed. For the solution of orbital problems of the general  $N$ -body problem, where multiple time-dependent frequencies are present, a new parameter  $u$  must be defined by estimating the actual frequency of the motion of any moving point mass.

For that, we consider the general case of  $N$  masses moving in three dimensions. If  $q_i(t)$  for  $i = 1, \dots, N$  is a representation of the  $i$ -th mass trajectory, its curvature can be computed as  $k_i(t) = \frac{\dot{q}_i(t) \times \ddot{q}_i(t)}{|\dot{q}_i(t)|^3}$ . The magnitude of the velocity of the  $i$ -th mass is  $|\dot{q}_i(t)|$ . After a time step  $h$ , the angular displacement of that mass is  $h|\dot{q}_i(t) \times \ddot{q}_i(t)|/|\dot{q}_i(t)|^2$ , which gives the following expression for each mass' actual frequency

$$\omega_i(t) = \frac{|\dot{q}_i(t) \times \ddot{q}_i(t)|}{|\dot{q}_i(t)|^2}. \quad (5)$$

For the specific case of physical problems that can be described using the Lagrangian  $L(q, \dot{q}) = \frac{1}{2}\dot{q}^T M(q)\dot{q} - V(q)$ , where  $M(q)$  is a symmetric positive definite mass matrix and  $V$  is a potential function, the continuous Euler-Lagrange equations are  $M(q)\ddot{q} = -\nabla V(q)$ . For that case, the frequency (5) for the  $i$ -th body at time  $t_k$ ,  $k = 1, \dots, N$  can be estimated as

$$\omega_i(t_k) = \frac{\left| M^{-1}(q_k)p_k \times \left( \frac{M^{-1}(q_k)p_k - M^{-1}(q_{k-1})p_{k-1}}{h} \right) \right|}{|M^{-1}(q_k)p_k|^2}, \quad (6)$$

where  $p_k$  is the conjugate momentum defined using the discrete Legendre transform [1]. The above frequency must also be estimated at the initial time  $t_0$  (with given initial positions and momenta  $\bar{q}_0$  and  $\bar{p}_0$  respectively), using the continuous Euler-Lagrange equation at that time we obtain

$$\omega_i(t_0) = \frac{\left| M^{-1}(\bar{q}_0)\bar{p}_0 \times (-M^{-1}(\bar{q}_0)\nabla V(\bar{q}_0)) \right|}{|M^{-1}(\bar{q}_0)\bar{p}_0|^2}. \quad (7)$$

Equations (6) and (7) yield an estimated frequency for each mass in general  $N$ -body problems.

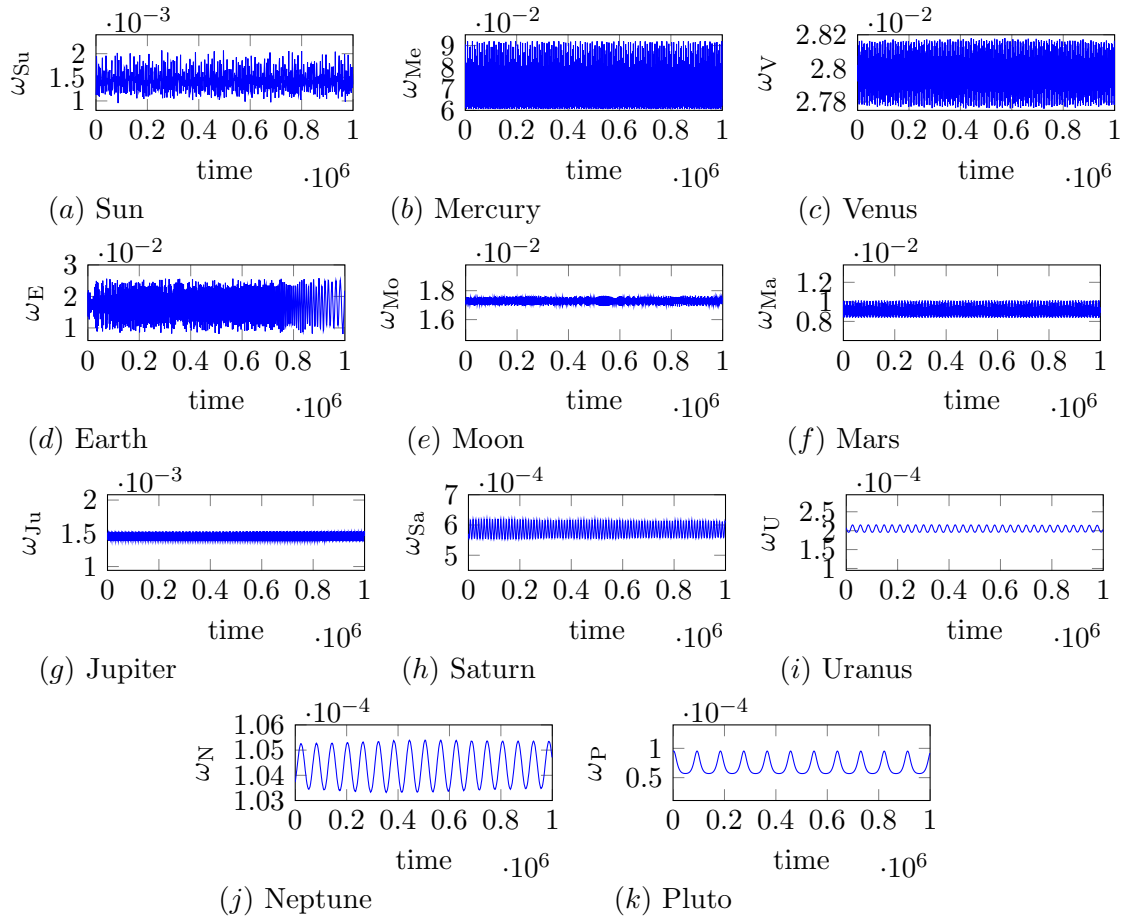


Figure 3: The estimated frequency (6) for the numerical integration of the complete solar system problem for  $10^6$  days, using trigonometric interpolation with  $S = 3$  and  $h = 1$  day for all the planets.

### Frequency estimation for the solar system problem

For a numerical test of frequency estimations in phase fitted variational integrators, the numerical solution of the complete solar system is regarded, i.e. the Lagrangian is  $L(q, \dot{q}) = \frac{1}{2} \sum_{i=1}^{11} m_i \dot{q}_i^2 + \sum_{i=1, j=1, i \neq j}^{11} G \frac{m_i m_j}{\|q_i - q_j\|}$  where  $G$  is the gravitational constant [2]. The estimated parameter  $\omega_i$ ,  $i = 1, \dots, 11$  at every time step is plotted in Figure 3. In that, even though the resulting frequency of the Sun's motion is not so stable (that comes from the type of the motion that Sun is following) for all other planets, the estimated frequency is remarkable stable, even for the  $10^6$  integration days. That frequency result arises from the elliptic orbit that planets are following subject to Sun's position.

Furthermore, Figure 5(a) shows the calculated positions of the planets using trigonometric interpolation functions using a time step equal to one day for  $S = 3$  intermediate points while Figure 5(b) shows the calculated positions for the Earth-Moon system. The gray shaded area represents the Moon's positions at every 10-th day. Although the results presented here are for  $10^6$  days and the time step is rather big (when compared to the period of motion of the planets close to Sun) the good behavior of the method can be observed. At last, for this numerical test, the evolution of the kinetic, potential and total energy of the system is shown in Figure 4, where it is clear that, even for long term integration processes, the energy behavior is good and stable.

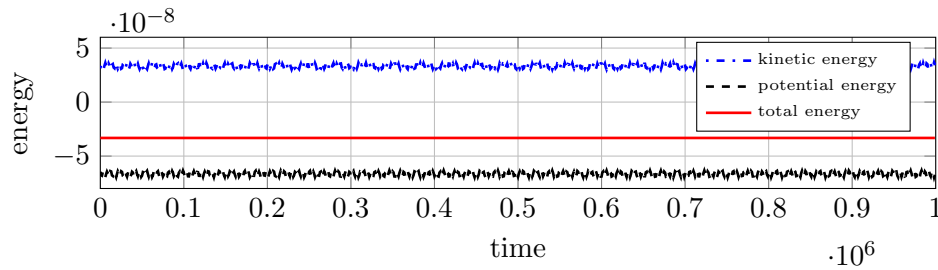


Figure 4: Kinetic, potential and total energy evolution for the numerical integration of the solar system problem for 1 million days, using trigonometric interpolation with  $S = 3$  and  $h = 1$  day.

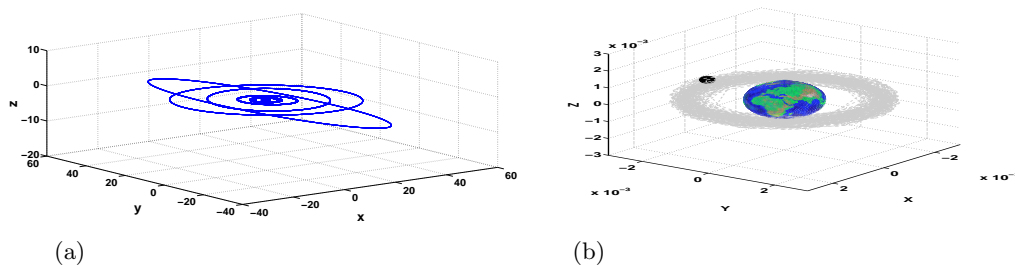


Figure 5: Orbits of the solar system problem for 1 million days using trigonometric interpolation techniques with  $h = 1$  day and  $S = 3$ . (a) The six outer planets. (b) Earth-Moon system.

## References

- [1] J.E. Marsden, and M. West. *Discrete mechanics and variational integrators*. Acta Numerica, Vol. 10, pp. 357-514, 2001.
- [2] E. Hairer, C. Lubich, and G. Wanner. *Geometric numerical integration illustrated by the Störmer/Verlet method*. Acta Numerica, Vol. 12, pp. 399-450, 2003.
- [3] O.T. Kosmas, and D.S. Vlachos. *Phase-fitted discrete Lagrangian integrators*. Computer Physics Communications, Vol. 181, pp. 562-568, 2010.
- [4] O.T. Kosmas, and S. Leyendecker. *Phase lag analysis of variational integrators using interpolation techniques*. PAMM Proc. Appl. Math. Mech, Vol. 12, pp. 677-678, 2012.
- [5] L. Brusca, and L. Nigro. *A one-step method for direct integration of structural dynamic equations*. Internat. J. Numer. Methods Eng, Vol. 15, pp. 685-699, 1980.
- [6] M. Leok, and J. Zhang. *Discrete Hamiltonian Variational Integrators*. IMA Journal of Numerical Analysis, Vol. 31, pp. 1497-1532, 2011.

## Computing time investigations of variational multirate systems

Tobias Gail, Sigrid Leyendecker, Sina Ober-Blöbaum

We investigate the behavior of variational multirate integration. For mechanical systems with dynamics on varying time scales, the numerical integration has to comply with contradicting requirements. On the one hand, to guarantee a stable integration of the fast motion, we need tiny step sizes. On the other hand, for the slow motions, a larger time step size is accurate enough. Furthermore, too small time steps increase the computing time unnecessarily, especially for costly function evaluations. For this, multirate systems split the system into subsystems [1] which can be solved with different methods [4]. For the multirate scheme we use two time step sizes in the framework described as variational multirate integration [3] which is developed on the basis of variational integrators [2] With this approach, we expect less computing time and demonstrate that this is the case by means of numerical examples. The example systems are the Fermi-Pasta-Ulam Problem (FPU) presented in Figure 2 and a simple atomistic model (SAM) illustrated in Figure 1, all consisting of multiple mass points and springs of varying stiffness while the latter one contains rigid links described by holonomic constraints. Let a mechanical system be described by a Lagrangian with a configuration vector  $q(t) \in Q \subseteq \mathbb{R}^n$  with  $Q$  a configuration manifold and a velocity vector  $\dot{q} \in TQ \subseteq \mathbb{R}^n$  on the tangent space  $TQ$ . Also, let the mechanical system be constrained by the  $m^c$ -dimensional holonomic function of constraints requiring  $g(q) = 0$ . Now, let the mechanical system contain fast and slow dynamics. Let this be characterized by the possibility to split the variables into  $n^s$  slow and  $n^f$  fast variables with  $q = (q^s, q^f)$  and  $n = n^s + n^f$ . Furthermore, we assume that we can split the potential energy into a slow potential  $V(q)$  and a fast potential  $W(q^f)$ . The action  $S$  is the time integral of the Lagrangian  $L(q, \dot{q}) = T(\dot{q}) - V(q) - W(q^f)$ . Via Hamilton's principle requiring stationarity of the action  $\delta S = 0$  the constrained multirate Euler-Lagrange equations are derived.

$$\begin{aligned} \frac{d}{dt} \frac{\partial T}{\partial \dot{q}^s} - \frac{\partial V}{\partial q^s} - \left( \frac{\partial g}{\partial q^s} \right)^T \cdot \lambda &= 0 \\ \frac{d}{dt} \frac{\partial T}{\partial \dot{q}^f} - \frac{\partial V}{\partial q^f} - \frac{\partial W}{\partial q^f} - \left( \frac{\partial g}{\partial q^f} \right)^T \cdot \lambda &= 0 \\ g(q) &= 0 \end{aligned} \tag{1}$$

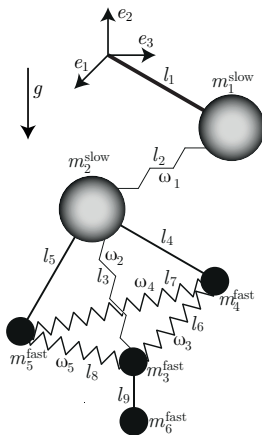


Figure 1: The simple atomistic model with slow and fast variables.

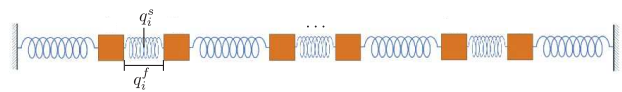


Figure 2: FPU with 6 masses and slow and fast variables.

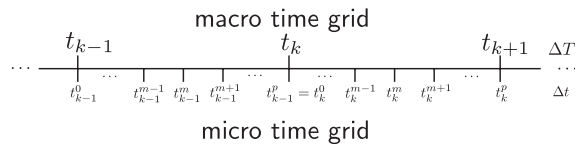


Figure 3: Macro and micro time grid.

Here  $T$  denotes the kinetic energy and  $\lambda$  the Lagrangian multiplier. To approximate the solution, rather than choosing one time grid we choose two time grids. Figure 3 shows such a time grid with macro time grid and micro time grid. Here, the macro time step is  $\Delta T$ , the micro time step is  $\Delta t$  and  $\Delta T \geq \Delta t$  holds.

The macro time grid provides the domain for the discrete slow variables  $q_d^s = \{q_k^s\}_{k=0}^N$  with  $q_k^s \approx q^s(t_k)$ , while the micro time grid provides the domain for the discrete fast variables  $q_d^f = \{\{q_k^{f,m}\}_{m=0}^p\}_{k=0}^{N-1}$  with  $q_k^{f,m} \approx q^f(t_k^m)$  and the discrete Lagrangian multipliers  $\lambda_d = \{\{\lambda_k^m\}_{m=0}^p\}_{k=0}^{N-1}$  with  $\lambda_k^m \approx \lambda(t_k^m)$ .

The discrete action  $S_d$  approximates the continuous action  $S$ . Via a discrete form of Hamilton's principle requiring stationarity for the discrete action, we derive the discrete constrained multirate Euler-Lagrange equations. These equations form a nonlinear set of equations which are solved using a Newton-Raphson method.

Quadrature rules are needed to approximate the action and constraints by discrete quantities. We use e.g. the midpoint rule, the trapezoidal rule, an affine combination and finite difference. Different quadrature rules can be chosen for the kinetic energy, both potential energies and lead to "fully implicit", "explicit slow, implicit fast" and "fully explicit" schemes.

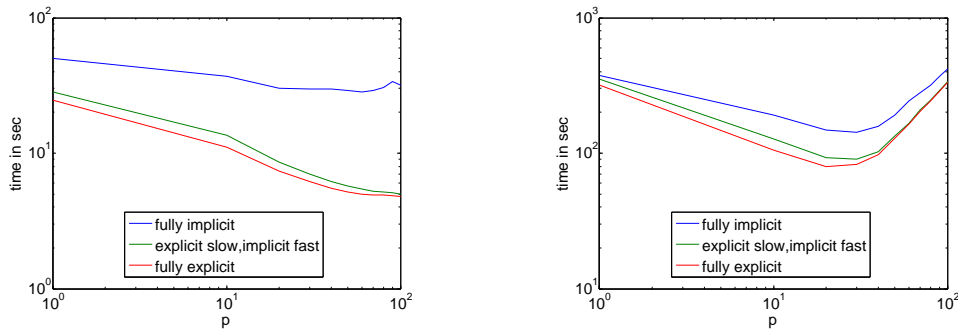


Figure 4: Computing time for fully implicit, explicit slow, implicit fast, and fully explicit schemes with  $p \in \{1, 10, 20, \dots, 100\}$  and  $dt = 0.01$  for FPU (left) and  $dt = 0.0001$  for SAM (right).

The computing time for the two mentioned examples is investigated. Figure 4 shows the computing times for the FPU and the SAM with all three quadrature schemes. In the figure we see that the computing times for both examples and all quadrature rules are decreasing with an increasing number of micro steps. Also one can see that for both examples the fully explicit scheme needs the least computing time. In both examples, the explicit slow, implicit fast and the fully explicit schemes perform better than the fully implicit scheme in terms of computing time.

As can be seen in Figure 4 there are limits to the savings, because for both systems there is a minimum computing time at a certain number of micro steps per macro step. The figure shows that for the SAM the minimum in computing time seems to be reached at a lower number of micro steps. Because the SAM has a larger number of degrees of freedom than the FPU, there seems to be a relation between the numbers of degrees of freedom and the minimum in computing time. To investigate this relationship, the FPU is used as a first example. Here, the number of degrees of freedom is the numbers of masses and can be easily varied. The number of masses is increased and the computing time is measured for different numbers of micro steps per macro step.

Figure 5 shows the computing time for different numbers of masses versus the number of micro steps for the FPU with three quadrature schemes. The left plot shows the computing times for the fully implicit scheme, the middle plot the explicit slow implicit fast scheme, and the right plot the fully explicit scheme. In all three plots it can be seen that the computing time minimum is at a lower number of micro steps with an increasing number of masses and therefore number of degrees of freedom. In

the left plot the minimum in computing time is for up to 90 masses at a number of micro steps  $p > 1$ . This means for up to 90 masses the fully implicit scheme has an advantage in computing time when introducing micro steps. For the middle plot the advantage in computing time when introducing micro steps is for up to 190 masses. The best performance here has the fully explicit scheme, because for over 220 masses the right plot shows an advantage in computing time when introducing micro steps.

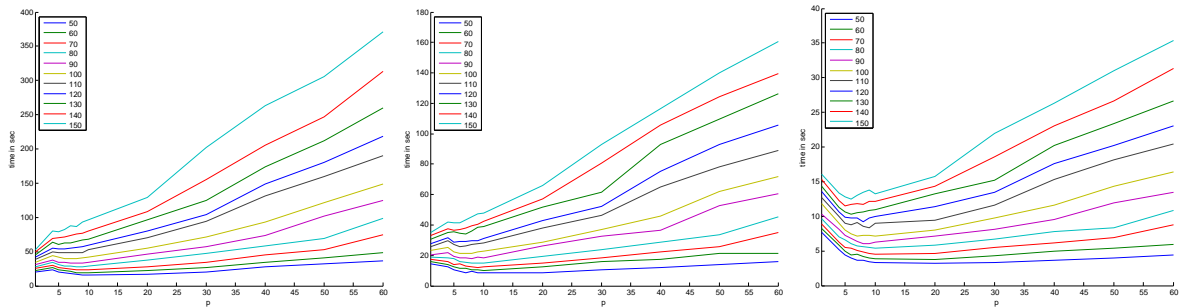


Figure 5: Computing time of the FPU with  $p \in \{1, 5, \dots, 12, 15, 19, 20, 30, \dots, 100\}$  and  $dt = 0.01$ .

## References

- [1] M. Arnold. *Multi-rate time integration for large scale multibody system models*. In P. Eberhard, editor, IUTAM Symposium on Multiscale Problems in Multibody System Contacts, Vol. 195(50-51), pp. 1-10, Springer, 2007.
- [2] A. Lew, J. E. Marsden, M. Ortiz, and M. West. *An overview of variational integrators*. In: L.P. Franca, T.E. Tezduyar and A. Masud (eds.), Finite Element Methods: 1970's and beyond, pp. 98-115, 2004.
- [3] S. Leyendecker, and S. Ober-Blöbaum. *A variational approach to multirate integration for constrained systems*. In: J.C. Samin, P. Fiset (eds.), Multibody Dynamics, Computational Methods in Applied Sciences, Vol. 28, pp. 97-121. Springer, 2013.
- [4] A. Stern, and E. Grinspun. *Implicit-explicit variational integration of highly oscillatory problems*. Multiscale Model. Simul., Vol. 7(4), pp. 1779-1794, 2009.

## Optimal control of standing high and long jumps

Michael W. Koch, Sigrid Leyendecker

The optimal control of human jumping and walking movements requires simulation techniques, which handle the contact's establishing and releasing between the foot and the ground. The investigated contact formulation covers the theory of perfectly plastic contacts. A direct transcription method, called DMOCC in [3], is used to transform the optimal control problem into a constrained optimisation problem. It involves a mechanical integrator based on a discrete constrained version of the Lagrange-d'Alembert principle. This integrator represents exactly the behavior of the analytical system concerning the consistency of momentum maps and symplecticity, therefore it is called a symplectic momentum scheme. To guarantee the structure preservation and the geometrical correctness during the establishing or releasing of the contact, the non-smooth problem is solved including the computation of the contact configuration, time and force, instead of relying on a smooth approximation of the

contact problem via a penalty potential.

The characteristics of human jumping are analysed using a simplified monopodal jumper, modelled as a three-dimensional constrained multibody system, to understand how the dynamics changes between the contact and the flight phase. The model consists of three rigid bodies, which represent the calf, the thigh and the upper part of the body. The human knee joint is modelled as a revolute joint, where the unit vector  $\mathbf{n}_1$  in body 2 represents the axis of rotation and the hip is modelled as a spherical joint. The constrained multibody system of the jumper is described by the configuration variable  $\mathbf{q} \in \mathbb{R}^k$ . Every rigid body is specified by a configuration vector  $\mathbf{q}^\alpha \in \mathbb{R}^{12}$ , composed by the placement of its center of mass and the right-handed director triad  $\mathbf{d}_i^\alpha(t)$  for  $i = 1, 2, 3$ . Accordingly,  $k$  equals 12 times the number of bodies. Due to the used rigid body formulation in use,  $m_{int} = 18$  internal constraints are present. The anatomical interconnections cause  $m_{ext} = 8$  external constraints and therefore the three-dimensional system is restricted by  $m = 26$  holonomic constraints. The  $k - m = 10$  generalised coordinates read  $\mathbf{u} = [\mathbf{u}^1 \ \boldsymbol{\theta}^1 \ \boldsymbol{\theta}_S \ \boldsymbol{\theta}_R] \in \mathbb{R}^{10}$ . In contrast to the oversimplified monopodal jumper in [2], the herein discussed jumper is actuated in the hip and the knee joint. The contact between the foot and the ground is modelled as perfectly plastic contact, which means, that during the contact phases the foot is fixed by the contact function  $\mathbf{g}_S = \mathbf{0} \in \mathbb{R}^3$  (spherical joint) at the ground. As a result of the constraints, the degrees of freedom are reduced to  $k - m - 3 = 7$ . The contact force immobilizes the jumper's foot and its function is to prevent the penetration of the ground. In this case, the third component of the contact Lagrange multiplier is negative ( $\lambda_{S_n}^3 < 0$ ) and more details are given in [2].

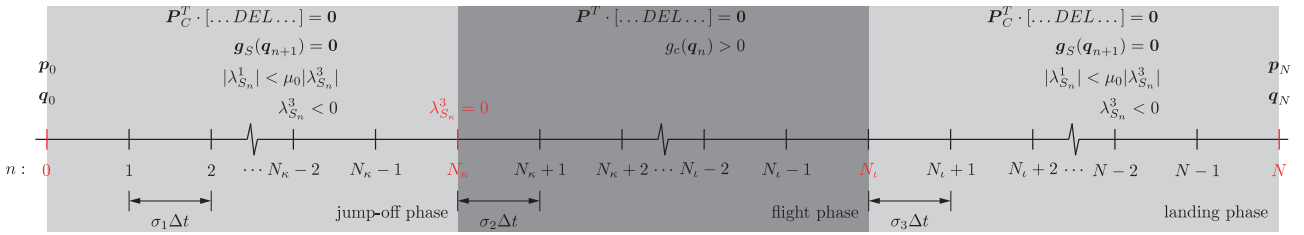


Figure 1: Time grid and dynamical constraints of the jumper's optimal control problem

The goal of the optimal control problem is to find the optimal trajectory and the optimal control sequence leading the monopodal jumper from an initial to a final state. A general illustration of the two optimal control problems of the standing high and long jumps is given in Figure 1.

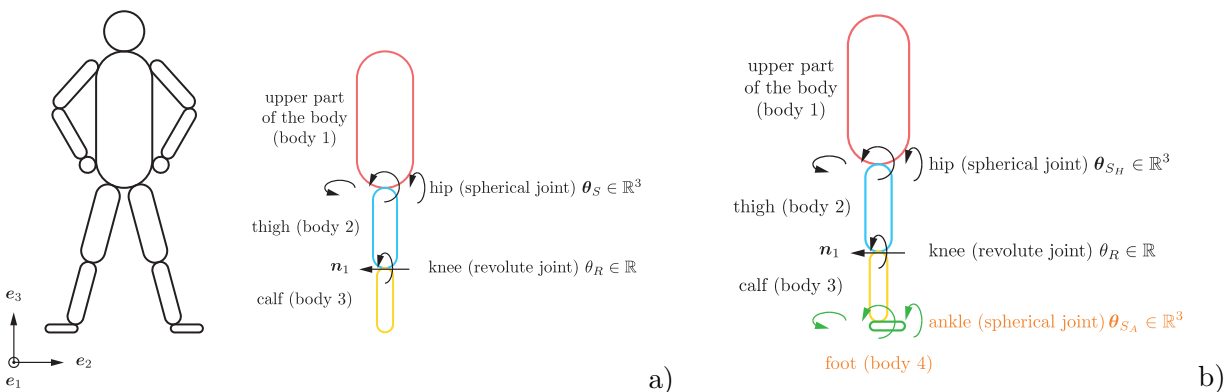


Figure 2: Model of the three-dimensional jumper neglecting the foot and its generalised coordinates in a) and in b) the more humanlike jumper model including the foot.

As shown, the motion consists of two contact phases, i.e. the jump-off phase at the beginning and the

landing phase at the end of the motion. The nodes  $N_\kappa$  and  $N_\ell$  represent the junction between the contact and the flight phase, so they are called switching points. The essential differences between the two jumping movements concerns the flight phase, whereby in the case of the long jump, the maximum length is required at the end of the flight phase. Considering the high jump movement, the maximum height is requested during the flight phase. The objective for the optimisation problems is to minimize the control effort, but the prospective goal is to investigate physiologically motivated cost functions, e.g. minimizing the joint forces during the landing phases and additional interesting objective functions are given in [1].

As illustrated in Figure 2 a), the foot is neglected in the first model, but the inclusion of the jumper's foot is a basic detail and it has enormous influence of the jumping movement before the contact between the foot and the ground is established or released. In a second model, the ankle is modelled as a spherical joint and the extended multibody system of the monopodal jumper is described by the configuration variable  $\mathbf{q} \in \mathbb{R}^{48}$ . As a result of the  $m_{int} = 24$  internal constraints and the  $m_{ext} = 11$  anatomical interconnections, the degrees of freedom are extended to  $k - m = 13$  and the generalised coordinates read  $\mathbf{u} = [\mathbf{u}^1 \ \boldsymbol{\theta}^1 \ \boldsymbol{\theta}_{S_H} \ \boldsymbol{\theta}_R \ \boldsymbol{\theta}_{S_A}] \in \mathbb{R}^{13}$ .

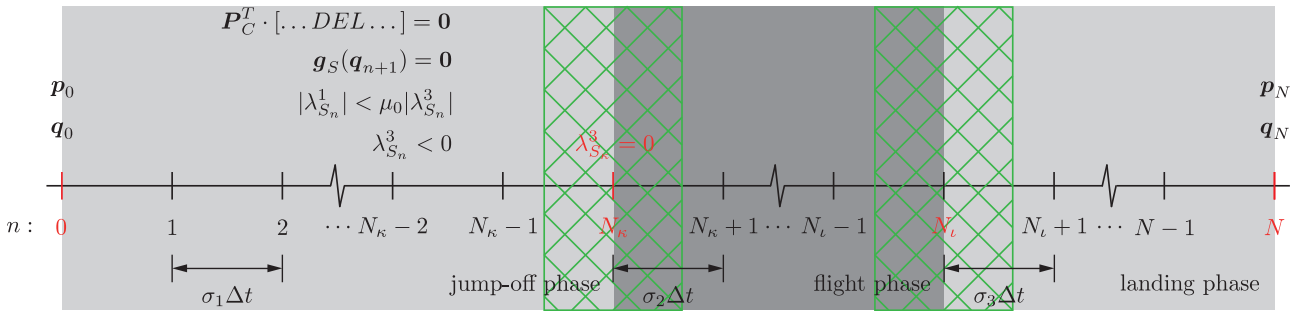


Figure 3: The time grid and the dynamical constraints of the extended optimal control problem.

As illustrated in Figure 3, the transition between the contact and the flight phases are enlarged to several switching points, in which sequentially the forefoot and the heel contact is established or released. According to these more humanlike adoptions, we expect that the results of the optimisation problem using the four-link monopodal jumper fit even better with the real human jumping movements.

## References

- [1] C. Dribusch, and S. Missoum. *Optimal Gait of two-dimensional gait*. Proceedings of the Multibody Dynamics 2011, ECCOMAS Thematic Conference, USB, Brussels, Belgium, 4-7 July 2011.
- [2] M. W. Koch, and S. Leyendecker. *Structure preservation simulation of monopodal jumping*. Archive of Mechanical Engineering, Vol. LX, pp. 127-146, 2013.
- [3] S. Leyendecker, S. Ober-Blöbaum, J.E. Marsden, and M. Ortiz. *Discrete mechanics and optimal control for constrained systems*. Computer Methods in Applied Mechanics and Engineering, Vol. 31 (1), pp. 505-528, 2009.

## Lie group variational integrators with quaternion parametrization of rotations

Thomas Leitz, Sigrid Leyendecker

The Lie group variational integrator presented here has the advantage that it uses a nonsingular representation of rotational degrees of freedom and at the same time doesn't require any constraints. This is accomplished by using a structure preserving variation of the action specific to rotations, rather than taking the directional derivative in any direction.

Instead of using elements of  $SO(3)$  as in [2], here rotations are represented by unit quaternions  $p \in \mathbb{H}^1 = \{p \in \mathbb{H} \mid \|p\| = 1\}$ . The material angular velocity is defined as  $\omega = 2\bar{p} \circ \dot{p} \in \mathbb{R}^3$ . We consider the Lagrangian  $L : \mathbb{H}^1 \times \mathbb{R}^3 \rightarrow \mathbb{R}$  as a function of orientation and angular velocity.

Variations of elements of  $\mathbb{H}^1$  are performed by applying the directional derivative using a one parameter subgroup element  $\exp(\varepsilon\eta) \in \mathbb{H}_\varepsilon^1 \subset \mathbb{H}^1$  where  $\varepsilon \in \mathbb{R}$ ,  $\eta \in \mathbb{R}^3$  and  $\exp(\cdot)$  is the quaternion exponential. The variations of the rotational position and the angular velocity then read

$$\delta p = \left. \frac{d}{d\varepsilon} \right|_{\varepsilon=0} p \circ \exp(\varepsilon\eta) = p \circ \eta \qquad \delta \omega = 2(\omega \times \eta + \dot{\eta})$$

We define a discrete Lagrangian (see [3]) as  $L_d^j : \mathbb{H}^1 \times \mathbb{H}^1 \rightarrow \mathbb{R}$  which approximates the action functional for one time step  $\Delta t^j = t^{j+1} - t^j$  where  $p^j \approx p(t^j)$  and  $f^j = \bar{p}^j \circ p^{j+1}$  is the rotational increment. The discrete action sum then reads

$$S_d = \sum_{j=1}^{N-1} L_d^j(p^j, f^j) \approx \int_0^T L(p, \omega) dt$$

Applying the discrete Hamilton's principle the discrete Euler-Lagrange equations are

$$a(f^j) = \Im \left( \bar{p}^j \circ \frac{\partial L_d^j}{\partial p^j} - \frac{\partial L_d^j}{\partial f^j} \circ \bar{f}^j + \bar{f}^{j-1} \circ \frac{\partial L_d^{j-1}}{\partial f^{j-1}} \right) = 0$$

Where  $a : \mathbb{H}^1 \rightarrow \mathbb{R}^3$ . Using the quaternion Cayley map  $\text{Cay} : \mathbb{R}^3 \rightarrow \mathbb{H}^1$  to express  $f^j = \text{Cay}(g^j)$ , the function  $a$  can locally be transformed into a function  $b : \mathbb{R}^3 \rightarrow \mathbb{R}^3$ , i.e.  $b(g) = 0$ , see [1]. These equations can be solved for  $g^j$  using a Newton-Raphson scheme and  $f^j$  is recovered using the Cayley map. The discrete Euler-Lagrange equations are derived for the physical pendulum with the discrete Lagrangian

$$L_d = \left( \frac{1}{2} (\omega^j)^T J \omega^j - mg\ell \langle p^j \circ e_3 \circ \bar{p}^j, e_3 \rangle \right) \Delta t$$

where  $m$  is the mass,  $g$  is the gravity constant,  $\ell$  is the length of pendulum,  $J$  is the  $4 \times 4$  inertia matrix and  $e_3 = [0, 0, 1]^T$ . Using the discretization of the angular velocity as

$$\omega^j := 2 \left( \frac{p^{j+1} + p^j}{2} \right) \circ \frac{p^{j+1} - p^j}{\Delta t} = \frac{1}{\Delta t} (f^j - \bar{f}^j) \in \mathbb{R}^3$$

results in the following discrete Euler-Lagrange equations

$$\Im [(Jf^j) \circ \bar{f}^j - (J\bar{f}^j) \circ \bar{f}^j] = \Im [\bar{f}^{j-1} \circ (Jf^{j-1}) - \bar{f}^{j-1} \circ (J\bar{f}^{j-1}) + \Delta t^2 mg\ell (\bar{p}^j \circ e_3 \circ p^j \circ e_3)]$$

Results of this integrator are compared to a variational integrator formulated on  $SO(3)$  for the parametrization of the rotational degrees of freedom and a similar approximation of the angular

velocity as in [2]. Figure 1 shows the evolution of the angle  $\varphi$  of the pendulum for a simple planar motion for the two integrators. One can observe, that the solution of the integrator formulated in terms of quaternions predicts a time of oscillation closer to the exact time  $T_{\text{exact}}$ . Figure 2 shows the energy behaviour typical for this type of integrator, i.e. there is no artificial change in total energy.

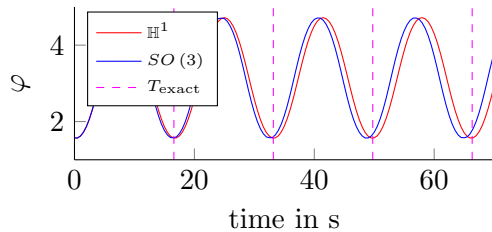


Figure 1: Evolution of the angle  $\varphi$ .

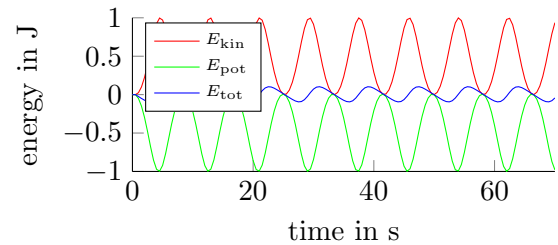


Figure 2: Energy behaviour of the integrator using quaternions.

## References

- [1] T. Lee. *Computational geometric mechanics and control of rigid bodies*. PhD thesis, University of Michigan, 2008.
- [2] T. Lee, N.H. McClamroch, and M. Leok. *A Lie group variational integrator for the attitude dynamics of a rigid body with applications to the 3D pendulum*. In Proceedings of 2005 IEEE Conference on Control Applications, pp. 962-967, 2005.
- [3] J.E. Marsden and M. West. *Discrete mechanics and variational integrators*. Acta Numerica, Vol. 10, pp. 357-514, 2001.

## On optimal control simulations of throwing

Ramona Maas, Sigrid Leyendecker

Human motion is investigated by means of numerical simulations from different viewpoints and with growing interest. Often, experimentally based inverse dynamics methods, supported by motion capturing measurements, as well as forward dynamics and optimal control simulations, e.g. extensively discussed in the context of human walking simulations in [4], are used within biomechanical investigations.

Within optimal control simulations, the goal is to find optimal trajectories and force fields that yield a motion, which is optimal in the sense of the defined objective function and which furthermore fulfils the equations of motion and possibly other constraints on the motion.

As an example, the problem of throwing with the goal of a maximal throwing distance is investigated during this work. In this context, we use a method called discrete mechanics and optimal control (DMOCC, see [2]), which benefits from the use of a variational integrator, guaranteeing that the solution of the optimal control problem inherits special characteristics of the real motion, like for example angular momentum consistency. Moreover, the solution does not suffer from any numerical drifts in the energy. In this work, the method is augmented by the implementation of muscle actuation. In the present human arm model, the elbow motion is generated by seven Hill-type muscle models, while the shoulder and the wrist are actuated by joint torques.

For the motion of a multibody system connected via joints and discretised with a constant time

step  $\Delta t \in \mathbb{R}$ , starting from a predefined initial configuration  $\mathbf{q}(t_0) = \mathbf{q}_0$  and conjugate momentum  $\mathbf{p}(t_0) = \mathbf{p}_0$  to a given end configuration  $\mathbf{q}(t_N) = \mathbf{q}_N$  and conjugate momentum  $\mathbf{p}(t_N) = \mathbf{p}_N$ , a typical optimal control problem is given in (1). Herein, an appropriate discrete objective  $J_d$ , with a discrete cost function  $C_d$ , is minimised and the discrete generalised coordinates  $\mathbf{u}_d = \{\mathbf{u}_n\}_{n=0}^N$ , the generalised joint torques  $\boldsymbol{\tau}_d^J = \{\boldsymbol{\tau}_n^J\}_{n=0}^{N-1}$  and the sequence of muscle activations  $\mathbf{A}_d = \{\mathbf{A}_n\}_{n=0}^{N-1}$  are the optimisation variables. At the same time, the symplectic-momentum consistent discrete equations of motion and boundary conditions (for example to start with zero momentum  $\mathbf{p}_0 = \mathbf{0}$ ) must be fulfilled. There may be further constraints like bounds on the optimisation variables and path constraints (equality or inequality), e.g. to set limits on the joint angles according to anatomical restrictions.

$$\min_{\mathbf{u}_d, \boldsymbol{\tau}_d^J, \mathbf{A}_d} J_d(\mathbf{u}_d, \boldsymbol{\tau}_d^J, \mathbf{A}_d) = \min_{\mathbf{u}_d, \boldsymbol{\tau}_d^J, \mathbf{A}_d} \sum_{n=0}^{N-1} C_d(\mathbf{u}_n, \mathbf{u}_{n+1}, \boldsymbol{\tau}_n^J, \mathbf{A}_n)$$

subject to: · fulfilment of the symplectic-momentum consistent discrete equations of motion (1)  
 · initial and final conditions  
 · path constraints

Within this numerical example, throwing with the goal of maximal throwing distance is examined using a human arm model. Hence, a goal has to be formulated that leads to a maximal throwing distance. When neglecting the air resistance and starting the throw from a height  $h = 0$ , the throw distance  $R$  can be calculated with  $R = \frac{v^2}{g} \sin(2\beta)$ . Herein,  $v$  is the throw velocity,  $g$  is the gravitational constant and  $\beta$  is the throw angle. This means, an appropriate objective for the optimisation problem is given by maximising  $v$  in direction of  $\beta = 45^\circ$ , represented by throw direction  $\mathbf{r}_d \in \mathbb{R}^3$ .

$$J_d(\mathbf{u}_d, \boldsymbol{\tau}_d^J, \mathbf{A}_d, \Delta t) = -\mathbf{r}_d^T \cdot \frac{\mathbf{q}_N^{\text{hand}} - \mathbf{q}_{N-1}^{\text{hand}}}{\Delta t} \quad (2)$$

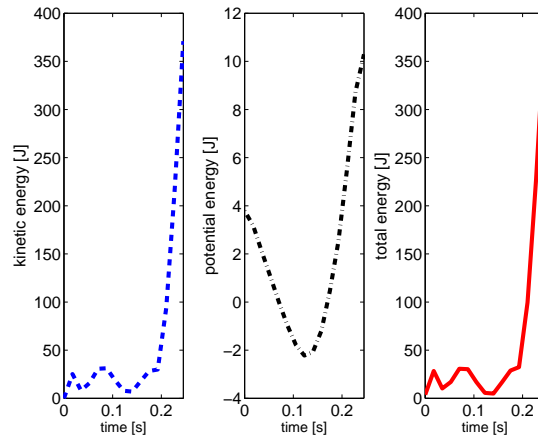


Figure 1: An optimal throwing motion: Evolution of kinetic, potential and total energy over time.

As this criterion does not affect the overall effort of the motion, it can yield physiologically not reasonable joint torque and muscle activity evolutions. Therefore, it is suggested to use this criterion together with a bound on the maximal effort of the motion.

The arm is fixed in space in the shoulder joint and the simulation starts from a predefined initial

arm position, as illustrated in the first plot of Figure 2, with an initial momentum  $\mathbf{p}_0 = \mathbf{0}$ . The end configuration is not strictly predefined but implemented via inequality constraints. They require an orientation of palm forward and a distance to the origin in the shoulder of minimal 0.2m in positive  $\mathbf{e}_2$ - and  $\mathbf{e}_3$ -direction at the end of the simulation time. Further inequality constraints are set on the joint angles in elbow and wrist via constraining the scalar products of the directors or via an approximation on the joint angle by summing up the generalised configuration variables. The simulation time is free, as the size of the time step  $\Delta t$  is included in the set of optimisation variables. The bounds on the time step size are set to  $[0.0175, 0.0225]$ s and the problem is discretised with  $N = 15$  time steps. In this simulation, the focus is on long throw, which is typically performed during sports education with a small, lightweight ball. To represent the mass of a ball, a point mass of 0.2kg is added to the hand's center of mass.

The resulting energy evolution over time, see Figure 1, shows a strong increase in kinetic and total energy with its maximum at the end of the motion, indicating that the final velocity is maximised, while the resulting optimal time step size is at its lower bound  $\Delta t = 0.0175$ s.

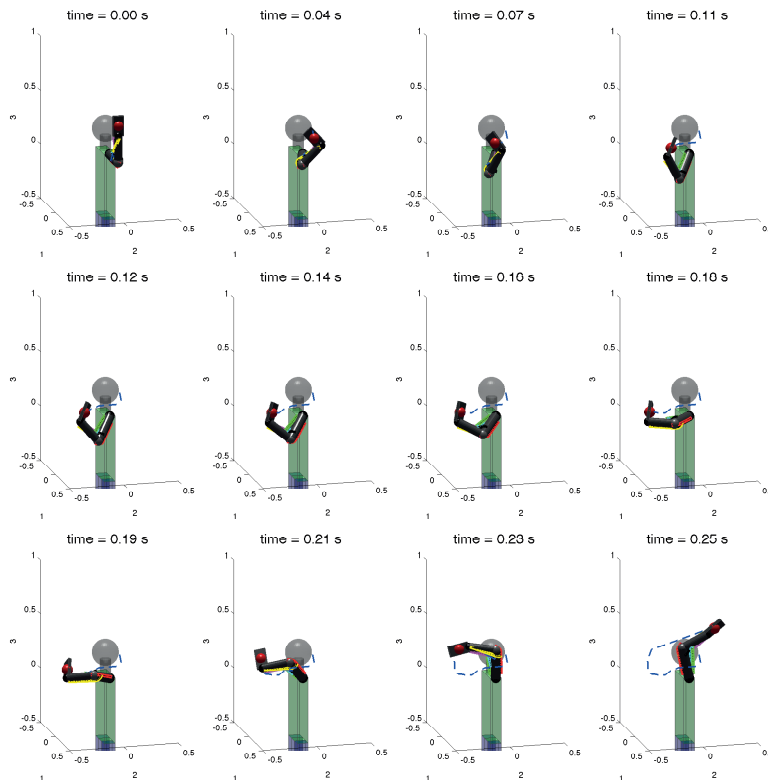


Figure 2: Snapshots of an optimal throwing motion.

It is generally known that during a throwing motion, momentum is gained by taking the arm far back in the beginning of the motion. Then, the arm is usually pulled fast forward like a pitch with the elbow ahead. The biomechanical principle behind optimal throwing motions is called 'principle of optimal acceleration distance', see [1]. It states that the longer a constant force acts on a body, the higher is the final velocity of this body. For throwing motions, this means there is an optimal backswing motion according to length and direction. However, the optimal trajectory of the throw is not necessarily the longest path. Excessive backswing motions can also be counterproductive, as muscles can be stretched over their optimal length, see for example [3]. Comparing this to the resulting motion of the optimal control simulation, see snapshots in Figure 2, a large coincidence can be found, in particular concerning the gaining of momentum by a posterior shoulder motion at the beginning of

the motion and the elbow being ahead during the final steps of the motion. However, there certainly exist differences to real throwing motions, as this optimal control simulation treats a standing throw, while typical throw motions are done with a run up and an additional twist of the upper body.

## References

- [1] G. Hochmuth. *Biomechanik sportlicher Bewegungen. (4. präzisierte und erweiterte Auflage)*. Sportverlag Berlin, 1981.
- [2] S. Leyendecker, S. Ober-Blöbaum, J.E. Marsden, and M. Ortiz. *Discrete mechanics and optimal control for constrained systems*. Optimal Control Applications and Methods, Vol. 31(6), pp. 505-528, 2009.
- [3] D. Scheibelhut. *Die Prinzipien der Biomechanik als Teil der Sportwissenschaft*. GRIN Verlag, 2010.
- [4] Y. Xiang, J. Arora, J., and K. Abdel-Malek. *Physics-based modeling and simulation of human walking: A review of optimization-based and other approaches*. Structural and Multidisciplinary Optimization, Vol. 42(1), pp. 1-23, 2010.

## Identifying various types of Pareto sets in multiobjective optimal control of multibody dynamics

Maik Ringkamp, Sina Ober-Blöbaum, Sigrid Leyendecker

Optimal control of multibody dynamics is present in a variety of practical applications e.g. robotics or biomechanics. The aim is to control the motion of rigid bodies such that some predefined objectives are optimized. For example, an industrial robot should move in minimal time, with minimal energy consumption, minimal mechanical wear and maximum payload and ideally, all objectives are optimized simultaneously. In the case of conflicting objectives, this is impossible because the optimal solution of one objective does not coincide with an optimal solution of another objective. In general, a decision maker has to select a trade-off solution that fits the specific demands best. Such problems are called *multiobjective optimal control problems* and the set of optimal trade-off solutions is the *Pareto set*. Figure 1 depicts the difference between the optimization of a single objective and the optimization of two objectives.

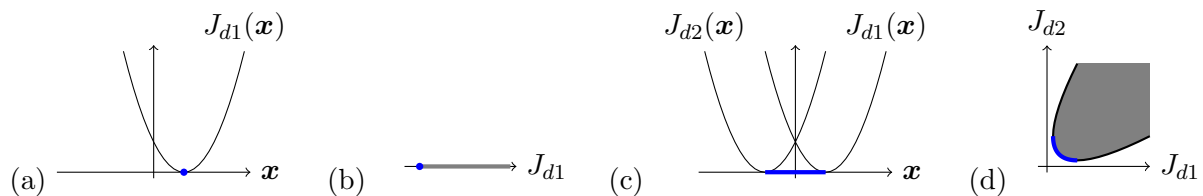


Figure 1: (a) The graph of a single objective  $J_{d1}$  and its optimal point in blue. (b) The image space of a single objective  $J_{d1}$ , its optimal value in blue, and its feasible set in gray. (c) The graph of two objectives  $J_{d1}$  and  $J_{d2}$  and their Pareto set in blue. (d) The image space of two objectives  $J_{d1}$  and  $J_{d2}$ , their Pareto front in blue, and their feasible set in gray.

## 1. Discretization of the multiobjective optimal control problem

The considered problem is a kinematic chain of four rigid bodies, interconnected by two revolute joints and one spherical joint (see Figure 2 and 3 (b)). The initial and final conditions (translation and rotation) are fully specified such that the kinematic chain moves from a straight to a closed position, performing a rest to rest maneuver in the presence of gravity. We minimize two objectives, the control effort for the entire maneuver and the required maneuver time, given here in discretized form:

$$J_{d1}(\mathbf{u}_d, \boldsymbol{\tau}_d, t_N) = \frac{t_N - t_0}{N} \sum_{i=0}^{N-1} \|\boldsymbol{\tau}_i\|^2 \quad (1)$$

$$J_{d2}(\mathbf{u}_d, \boldsymbol{\tau}_d, t_N) = t_N \quad (2)$$

The multiobjective optimal control problem is transformed to a discretized formulation via a direct discretization approach called DMOCC [2]. DMOCC is a combination of Discrete Mechanics and Optimal Control (DMOC) [3] and discrete versions of the reparametrization to generalized parameters and a null space method [4]. Instead of discretizing the Euler-Lagrange equations of motion directly, we use a discrete variational principle. In the following, we sketch the main idea and refer to [2] for details.

The time interval  $[t_0, t_N]$  is replaced by a set of  $N + 1$  equidistant time nodes  $t_0 \leq t_1 \leq \dots \leq t_N$  with  $t_i = t_0 + ih, i \in [N] := \{0, 1, \dots, N\}$  and a step size  $h = \frac{t_N - t_0}{N}$ . The configuration functions  $\mathbf{q} : [t_0, t_N] \rightarrow Q, \mathbf{u} : [t_0, t_N] \rightarrow U$  are replaced by a value at each time node, leading to discrete functions  $\mathbf{q}_d : \{t_i | i \in [N]\} \rightarrow Q$  and  $\mathbf{u}_d : \{t_i | i \in [N]\} \rightarrow U$ , with  $\mathbf{q}_i := \mathbf{q}_d(t_i) \approx \mathbf{q}(t_i)$  and  $\mathbf{u}_i := \mathbf{u}_d(t_i) \approx \mathbf{u}(t_i)$ . Similarly, the discrete control function  $\boldsymbol{\tau}_d$  approximates the continuous control function on each interval  $[t_i, t_{i+1}]$ . Finite differences and numerical integration are used to replace  $TQ$  by  $Q \times Q$  and to discretize the Lagrange-d'Alembert principle based on a discrete Lagrangian  $L_d : Q \times Q \rightarrow \mathbb{R}$ . Taking discrete variations  $\delta \mathbf{q}_i, i \in [N]$  leads to discrete Euler-Lagrange equations that approximate the equations of motion.

Similar as in [2], a discrete reparametrization  $\mathbf{F}_d : U \times Q \rightarrow C$  with  $\mathbf{q}_i = \mathbf{F}_d(\mathbf{u}_i, \mathbf{q}_{i-1})$ , a null space matrix  $\mathbf{P}_d^T(\mathbf{q}_i)$  and an input transformation matrix  $\mathbf{B}_d^T(\mathbf{q}_i)$  are used to reduce the dimension. The reduced scheme reads

$$\mathbf{P}_d^T(\mathbf{q}_i) \left[ D_2 L_d(\mathbf{q}_{i-1}, \mathbf{q}_i) + D_1 L_d(\mathbf{q}_i, \mathbf{F}_d(\mathbf{u}_{i+1}, \mathbf{q}_i)) + \frac{h}{2} \mathbf{B}_d^T(\mathbf{q}_i) (\boldsymbol{\tau}_{i-1} + \boldsymbol{\tau}_i) \right] = \mathbf{0} \quad (3)$$

for  $i = 1, \dots, N - 1$ . In the same way, we obtain discretized versions of the initial and final conditions (4), (5), and lower and upper bounds (6) with  $t_0 < \underline{t}_N$ .

$$\mathbf{r}_{d0}(\mathbf{u}_0, \mathbf{u}_1, \boldsymbol{\tau}_0) = \mathbf{0} \quad (4)$$

$$\mathbf{r}_{dN}(\mathbf{u}_{N-1}, \mathbf{u}_N, \boldsymbol{\tau}_{N-1}) = \mathbf{0} \quad (5)$$

$$\underline{\mathbf{u}}_d \leq \mathbf{u}_d \leq \overline{\mathbf{u}}_d, \quad \underline{\boldsymbol{\tau}}_d \leq \boldsymbol{\tau}_d \leq \overline{\boldsymbol{\tau}}_d, \quad \text{and} \quad \underline{t}_N \leq t_N \leq \overline{t}_N \quad (6)$$

## 2. Computation of the Pareto set

The feasible set  $S$  is defined by equations (3)-(6) of the underlying discretized multiobjective optimal control problem. One way to approximate it is to use slack variables to transform the inequality constraints into additional equality constraints. The resulting problem is a root finding problem and can be solved e.g. by using global subdivision techniques [5], or locally by continuation methods as similarly done in [6].

As we are interested in a rather rough approximation, we use a simpler approach here. First, we

randomly select a finite number of possibly infeasible trajectories  $\mathbf{x}$  that satisfy the lower and upper bounds (6). These are initial guesses for the minimization problem  $\min_{\mathbf{x} \in S} 1$  leading to a finite set of trajectories  $S_d \subseteq S$ . Moreover, evaluating  $\mathbf{J}$  on each feasible point leads to a finite approximation of the image of the feasible set  $\mathbf{J}(S)$  such that we have  $S_d \approx S$  and  $\mathbf{J}(S_d) \approx \mathbf{J}(S)$ . Further, applying a test of dominance on these sets leads to an approximation of the Pareto set and front  $\mathcal{P}_d \approx \mathcal{P}$  and  $\mathbf{J}(\mathcal{P}_d) \approx \mathbf{J}(\mathcal{P})$ . Depending on the number of the initially selected trajectories, this approximation can be quite rough. However,  $\mathbf{J}(\mathcal{P}_d)$  already indicates the shape of the Pareto front which is used to determine an appropriate scaling of the objective function and provides initial guesses for the later used reference point method (for details see [7]).

### 3. Numerical Results

The method is implemented in Matlab and uses ADiMat [8] algorithmic differentiation for the computation of the sparse Jacobian of the nonlinear constraint function defined by (3)-(5).

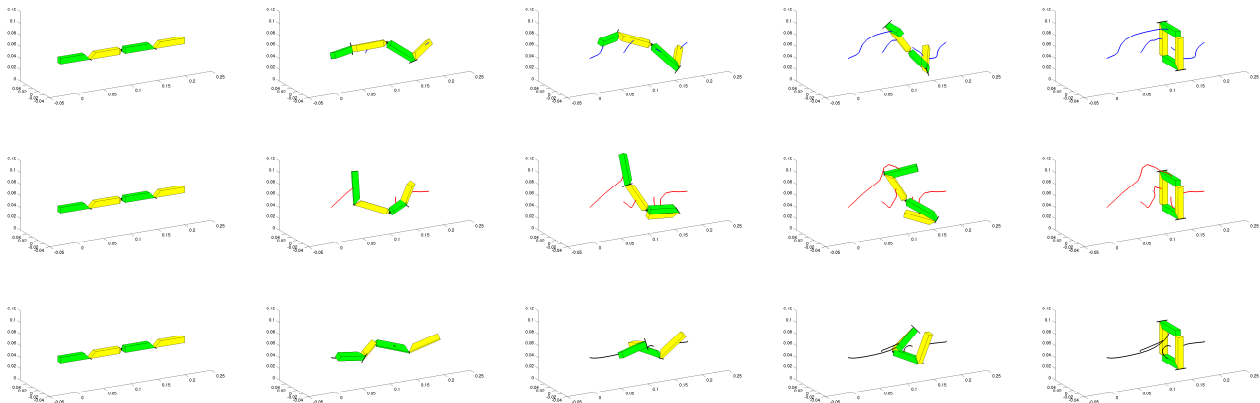


Figure 2: Selected movements for three types of Pareto optimal trajectories of the four body kinematic chain at the time nodes: 1, 5, 8, 11 and 15. Trajectories with  $\mathbf{J}_d = (0.1681, 0.0286)$  in blue in the first row, with  $\mathbf{J}_d = (0.1834, 0.0283)$  in red in the second row, and with  $\mathbf{J}_d = (0.1500, 0.0296)$  in black in the third row.

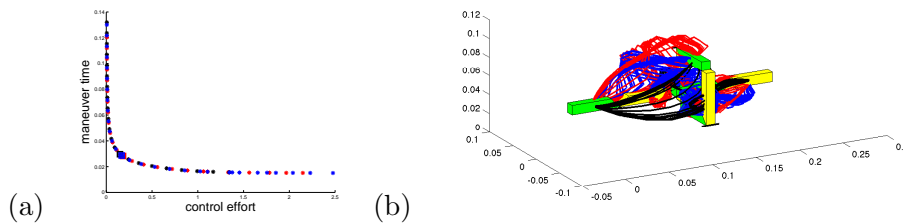


Figure 3: (a) Objective space, Pareto front (blue, red, and black stars) for different types of trajectories. Movements of selected Pareto points for each type (blue, red, and black squares) are given in Figure 2. (b) Three types of Pareto optimal trajectories of the four body kinematic chain for each type.

In order to compute a rough approximation of the feasible set, we use SQP to solve  $\min_{\mathbf{x} \in S} 1$  with random initial guesses, each of them already fulfilling the lower and upper bounds. Using various stricter bounds can help to yield a better approximation, at least for the considered example. The rough approximation is used to scale the objectives and three distinct points are selected as initial guesses for a reference point method. This finally leads to an approximation of the Pareto set depicted in Figure 3 (a) in blue, red and black. Each Pareto point is colored according to the corresponding starting point of the continuation. Three types of different trajectories can be detected in the space of the redundant coordinates (Figure 3 (b) in blue, red, and black). The movement is depicted exemplary in Figure 2 for selected trajectories with  $\mathbf{J}_d = (0.1681, 0.0286)$  in blue,  $\mathbf{J}_d = (0.1834, 0.0283)$  in red, and  $\mathbf{J}_d = (0.1500, 0.0296)$  in black and the corresponding Pareto points are highlighted in Figure 3 (a). Probably these types represent local smooth connected parts of the Pareto set.

## References

- [1] T.S. Ratiu, and J.E. Marsden. *Introduction to mechanics and symmetry*. Springer, 2010.
- [2] S. Leyendecker, S. Ober-Blöbaum, J. E. Marsden, and M. Ortiz. *Discrete Mechanics and optimal control for constrained systems*. Optimal Control, Applications and Methods, Vol. 31(6), pp. 505-528, 2010.
- [3] S. Ober-Blöbaum, O. Junge, and J.E. Marsden. *Discrete mechanics and optimal control: an analysis*. Control, Optimisation and Calculus of Variations, Vol. 17(2), pp. 322-352, 2011.
- [4] S. Leyendecker, J.E. Marsden, and M. Ortiz. *Variational integrators for constrained dynamical systems*. ZAMM-Journal of Applied Mathematics and Mechanics/Zeitschrift für Angewandte Mathematik und Mechanik, Vol. 88(9), pp. 677-708, 2008.
- [5] M. Dellnitz, O. Schütze, and S. Sertl. *Finding zeros by multilevel subdivision techniques*. IMA Journal of Numerical Analysis, Vol. 22(2), pp. 167-185, 2002.
- [6] M. Ringkamp, A. Walther, P. Reinold, K. Witting, M. Dellnitz, and A. Traechtler. *Using Algorithmic Differentiation for the Multiobjective Optimization of a Test Vehicle*. EVOLVE, A bridge between Probability, Set Oriented Numerics and Evolutionary Computation, DVD, Mexico City, Mexico, 2012.
- [7] M. Ringkamp, S. Ober-Blöbaum, and S. Leyendecker. *A numerical approach to multiobjective optimal control of multibody dynamics* Proceedings of the ECCOMAS Thematic Conference on Multibody Dynamics, DVD, Zagreb, Croatia, 2013.
- [8] C.H. Bischof, H.M. Bücker, B. Lang, A. Rasch, and A. Vehreschild. *Combining Source Transformation and Operator Overloading Techniques to Compute Derivatives for MATLAB Programs*. Proceedings of the Second IEEE International Workshop on Source Code Analysis and Manipulation (SCAM 2002), pp. 65-72, 2002

## Finite element modelling of dielectric elastomers

Tristan Schlögl, Sigrid Leyendecker

Modern robotic systems suffer some severe dynamic limitations. The rigid coupling between electrical drives and joints does not allow for dynamic motions like they occur in nature, where muscles act as an energy buffer and store energy. However, this elastic behaviour plays an important role when considering humanoid systems in terms of safety, energy efficiency and robustness.

Dielectric elastomer actuators are composed of a series of elastic capacitors, each one equipped with two conductive layers separated by an insulating material with small Young's modulus and large permittivity [1]. In this collaborative work [2] a dielectric silicone is used as the main component and conductive layers are introduced by adding carbon nanotubes. The structure of a single actuator cell is illustrated in Figure 1 on the left hand side. As with capacitors, when an external voltage is applied to the conductive layers, an electric field is established. To be observed in Figure 1 on the right hand side, electrostrictive effects then lead to a contraction of the silicone, as dipoles and other polarisation types caused by the electric excitation are formed.

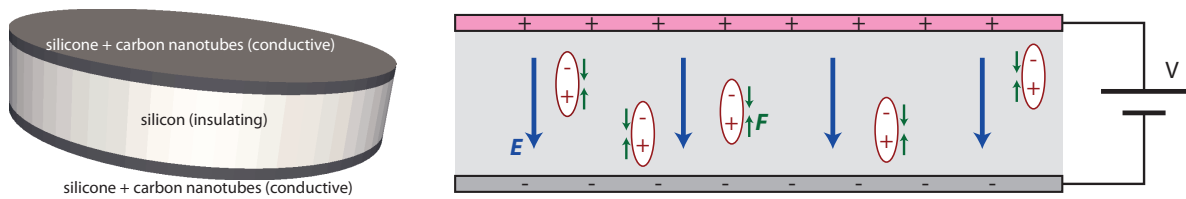


Figure 1: Three layer structure of a dielectric elastomer actuator (left) and electrostriction (right).

These effects can be described by the Maxwell equations, the balance of momentum and constitutive material laws. Assuming that the electric field can be regarded as quasi-static, no external magnetic fields are applied and no free currents and electric charges are present, electrostatics are covered by [3]

$$\nabla_{\mathbf{X}} \times \mathbf{E} = \mathbf{0}, \quad (1)$$

with the electric field vector  $\mathbf{E}$  in the reference configuration  $\mathbf{X} \in \mathcal{B}_0$  and

$$\nabla_{\mathbf{X}} \cdot \mathbf{D} = 0, \quad (2)$$

where  $\mathbf{D}$  is the electric displacement vector in the reference configuration. From equation (1) it directly follows that  $\mathbf{E}$  is conservative and can be expressed as the gradient of a scalar electric potential  $\varphi$  by

$$\mathbf{E} = -\nabla_{\mathbf{X}} \varphi. \quad (3)$$

Note that additional boundary terms are needed in order to solve the equations. Vectors in the reference configuration are obtained by the pull-back operations  $\mathbf{E} = \mathbf{F}^T \cdot \mathbf{e}$  and  $\mathbf{D} = J\mathbf{F}^{-1} \cdot \mathbf{d}$  for the electric field  $\mathbf{e}$  and the electric displacement  $\mathbf{d}$  in the spatial configuration, using the deformation gradient  $\mathbf{F}$  and its determinant  $J = \det(\mathbf{F})$ .

The balance of momentum is given by [4]

$$\nabla_{\mathbf{X}} \cdot \mathbf{P}^T + \mathbf{f}_e = \rho_0 \ddot{\mathbf{x}}, \quad (4)$$

where  $\mathbf{P}$  is the Piola-Kirchhoff stress tensor,  $\mathbf{f}_e$  is the force resulting from electrostatics,  $\rho_0$  is the mass density in the reference configuration and  $\ddot{\mathbf{x}}$  is the absolute acceleration of a spatial point. Together with the definition [3]

$$\mathbf{D} = \varepsilon_0 J \mathbf{C}^{-1} \cdot \mathbf{E} + \mathbf{P}^{\text{el}}, \quad (5)$$

where  $\mathbf{C}$  is the right Cauchy-Green tensor,  $\mathbf{P}^{\text{el}}$  is the material polarisation vector and  $\varepsilon_0$  is the vacuum permittivity, and the electric body force given by [5]

$$\mathbf{f}_e = \nabla_{\mathbf{X}} (\mathbf{F}^{-T} \cdot \mathbf{E}) \cdot \mathbf{P}^{\text{el}}, \quad (6)$$

equation (4) can be rewritten as

$$\nabla_{\mathbf{X}} \cdot \mathbf{T}^T = \rho_0 \ddot{\mathbf{x}}, \quad (7)$$

with the total stress  $\mathbf{T}$  being superposed of  $\mathbf{P}$  and some electric counterpart. Note that for an actual simulation, equation (7) needs to be completed by initial and boundary conditions.

By integrating the energy function

$$\Omega(\mathbf{F}, \mathbf{E}) = \underbrace{\frac{\mu}{2}[\mathbf{C} : \mathbf{1} - 3] - \mu \ln(J) + \frac{\lambda}{2}[\ln(J)]^2}_{\text{Neo-Hooke}} + \underbrace{c_1 \mathbf{E} \cdot \mathbf{E}}_{\text{electric}} + \underbrace{c_2 \mathbf{C} : [\mathbf{E} \otimes \mathbf{E}] - \frac{1}{2} \varepsilon_0 J \mathbf{C}^{-1} : [\mathbf{E} \otimes \mathbf{E}]}_{\text{coupling}} \quad (8)$$

with Lamé parameters  $\mu$  and  $\lambda$ , electric parameters  $c_1$  and  $c_2$  and the identity  $\mathbf{1}$  over the material body  $\mathcal{B}_0$ , an expression for the potential energy  $V$  is obtained. Together with the kinetic energy

$$T = \int_{\mathcal{B}_0} \frac{1}{2} \rho_0 \|\dot{\mathbf{x}}\|^2 dV, \quad (9)$$

the Lagrange function

$$L = T - V \quad (10)$$

can be evaluated. By following Hamilton's principle

$$\delta S = 0 \quad (11)$$

and requiring that the first variation of the action integral

$$S = \int_{t_0}^{t_1} L dt \quad (12)$$

vanishes, after some calculation equation (7) is recovered, meaning that equation (11) based on  $T$  and  $V$  is equivalent to equation (7).

Approximating the action integral using quadrature rules, discretising with finite elements in space and finite differences in time and applying Hamilton's principle (11) for the discrete set of equations, structure preserving integration schemes, generally non-linear and implicit, of the form

$$\underline{\underline{M}} \frac{1}{\Delta t^2} \cdot (\underline{x}^{n+1} - 2\underline{x}^n + \underline{x}^{n-1}) + \underline{R}(\underline{x}^{n+1}, \underline{x}^n, \underline{x}^{n-1}) = \underline{0} \quad (13)$$

with the time index  $n$ , state variables  $\underline{x}$  and non-linear terms  $\underline{R}$  are obtained [6]. Note that, due to the fact that electrodynamic effects are not considered here, the entries of the mass matrix  $\underline{\underline{M}}$  associated with electric degrees of freedom are zero. Using a Newton-Raphson scheme and providing initial values, boundary conditions as well as certain quadrature rules when developing the discrete Lagrangian, this non-linear problem can be solved for unknown displacements and electric potentials at each finite element node. Figure 2 illustrates the results of an in-house MATLAB FEM solver, evaluating the quasi-static state of a given muscle shape for applied voltage.

This model forms the basis for future work regarding optimal control problems, where DEAs are used as actuators in robotics.

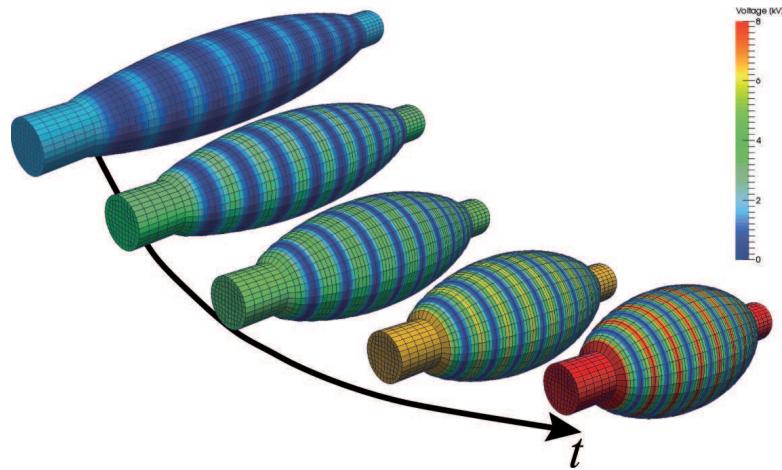


Figure 2: Contraction of a dielectric elastomer actuator in muscle shape due to an applied voltage.

### References

- [1] Y. Bar-Cohen. *Electroactive polymers as artificial muscles – capabilities, potentials and challenges*. Handbook on biomimetics, Section 11, Chapter 8, 2000.
- [2] S. Reitelshöfer, M. Landgraf, T. Schlögl, J. Franke, and S. Leyendecker. *Qualifying dielectric elastomer actuators for usage in complex and compliant robot kinematics*. Poster, International conference on Electromechanically Active Polymer (EAP) transducers & artificial muscles, Dübendorf, Switzerland, 25-26 June 2013.
- [3] D.K. Vu, P. Steinmann, and G. Possart. *Numerical modelling of non-linear electroelasticity*. International Journal for Numerical Methods in Engineering, Vol. 70, pp. 685-704, 2006.
- [4] P.G. Ciarlet. *Mathematical Elasticity*. Elsevier, 2004
- [5] Y.H. Pao. *Electromagnetic forces in deformable continua*. Mechanics Today, Vol. 4. pp. 209-306, 1978.
- [6] J.E. Marsden, and M. West. *Discrete mechanics and variational integrators*. Acta Numerica, Vol. 10, pp. 357-514, 2001.

## 4 Activities

### 4.1 Teaching

#### Wintersemester 2013/2014

Biomechanik der Bewegung (MT) Vorlesung + Übung	H. Lang
Dynamik starrer Körper (MB, ME, WING, IP, BPT, CE) Vorlesung Übung + Tutorium	S. Leyendecker O.T. Kosmas, T. Leitz M. Ringkamp, T. Schlögl
Mehrkörperdynamik (MB, ME, WING, TM, BPT, CE) Vorlesung Übung	S. Leyendecker H. Lang
Numerische Methoden in der Mechanik (MB, ME, WING, TM, BPT) Vorlesung + Übung	H. Lang
Theoretische Dynamik I (MB, ME, WING, TM, CE, BPT) Vorlesung + Übung	H. Lang

#### Sommersemester 2013

Statik und Festigkeitslehre (CBI, CE, ET, LSE, ME, MWT, IP, MT, CEN, BPT) Vorlesung Übung + Tutorium	S. Leyendecker T. Gail, T. Leitz, O.T. Kosmas R. Maas, M. Ringkamp
geprüft	377
Biomechanik (MT) Vorlesung + Übung geprüft	H. Lang
	90 + 12 (WS 12/13)
Geometrische Mechanik und geometrische Integratoren (MB, ME, WING) Vorlesung Übung geprüft	S. Leyendecker H. Lang
	5
Theoretische Dynamik II (M, TM, MB, ME, CE, BPT, WING, Ph) Vorlesung + Übung geprüft	H. Lang
	8
Dynamik nichtlinearer Balken (MB, M, Ph, CE, ME, WING) Vorlesung geprüft	H. Lang
	4

Rechnerunterstützte Produktentwicklung (RPE)  
Versuch 6: Mehrkörpersimulation in Simulink  
(MB, ME, WING) Praktikum

M. Koch, O.T. Kosmas  
T. Leitz, R. Maas, M. Ringkamp

Teilnehmer 70

### Wintersemester 2012/2013

Dynamik starrer Körper (MB, ME, WING, IP, BPT, CE)

Vorlesung

S. Leyendecker

Übung + Tutorium

T. Gail, O.T. Kosmas

T. Leitz, M. Ringkamp

geprüft 564 + 155 (SS 2013)

Mehrkörperdynamik (MB, ME, WING, TM, BPT, CE)

Vorlesung

S. Leyendecker

Übung

H. Lang

geprüft 35 + 3 (SS 2013)

Theoretische Dynamik I (MB, ME, WING, TM, CE, BPT)

Vorlesung + Übung

H. Lang

geprüft 12 + 2 (SS 2013)

Numerische Methoden in der Mechanik (MB, ME, WING, TM, CE, BPT)

Vorlesung + Übung

H. Lang

geprüft 14 + 3 (SS 2013)

Dynamik nichtlinearer Balken (MB, M, Ph, CE, ME, WING)

Vorlesung

H. Lang

geprüft 6

## 4.2 Seminar for Mechanics

### together with the Chair of Applied Mechanics LTM

21.01.2013 Steffen Göbel

Federal Mogul Nuremberg, Germany

*Topologieoptimierung des Radträgers eines Formula Student Rennwagens*

23.01.2013 Odysseas Kosmas

Chair of Applied Dynamics, FAU Erlangen-Nuremberg, Germany

*Phase fitted variational integrators using interpolation techniques for the general N-body problem*

23.01.2013 Saskia Sitzmann

ZISC Erlangen, Germany

*Mortar contact in the FEM package CalculiX*

- 26.04.2013 Olivier A. Bauchau  
University of Michigan – Shanghai Jiao Tong University Joint Institute, China  
*Three-dimensional beam theory for flexible multibody dynamics*
- 27.05.2013 Stefan Sandfeld  
Institute of Materials Simulation (WW8), Department of Materials Science, FAU  
Erlangen-Nuremberg, Germany  
*From systems of discrete dislocations to a continuous field representations: the continuum dislocation dynamics theory*
- 21.06.2013 Dominik Budday  
Karlsruhe Institute of Technology, Germany  
*Analyse des räumlichen Gehens anhand eines Masse-Feder Modells*
- 08.07.2013 Thomas Graupeter  
Lehrstuhl für Systemsimulation, Department Informatik, FAU Erlangen-Nuremberg,  
Germany  
*Birefringence in solid-state laser rods due to the thermal lensing effect regarding shear strains in axial-radial plane*
- 19.07.2013 Bernhard Eidel  
Institut für Mechanik, Universität Duisburg-Essen, Germany  
*On atomistic-continuum coupling for crystalline nano-structures: from surface relaxations to localized inelastic mechanisms*
- 26.09.2013 Thorsten Brand  
Erlangen Centre for Astroparticle Physics, FAU Erlangen-Nuremberg, Germany  
*An automated data reduction pipeline for the Hartebeesthoek Radio Astronomy Observatory*
- 09.10.2013 Winnifried Wollner  
Fakultät für Mathematik, Informatik und Naturwissenschaften, Universität Hamburg,  
Germany  
*DOPelib – a differential equations and optimization toolkit*
- 02.12.2013 Markus Härtel  
TU Chemnitz, Germany  
*Auf der Suche nach der äquivalenten Querschnittsfläche – Simulation eines Kreuzzugversuches*
- 11.12.2013 George Chatzigeorgiou  
Arts et Métiers ParisTech, Metz, France  
*Theoretical and computational aspects on surface electrostatics*

### 4.3 Dynamics laboratory

Tristan Schlögl, Nathanael Bach

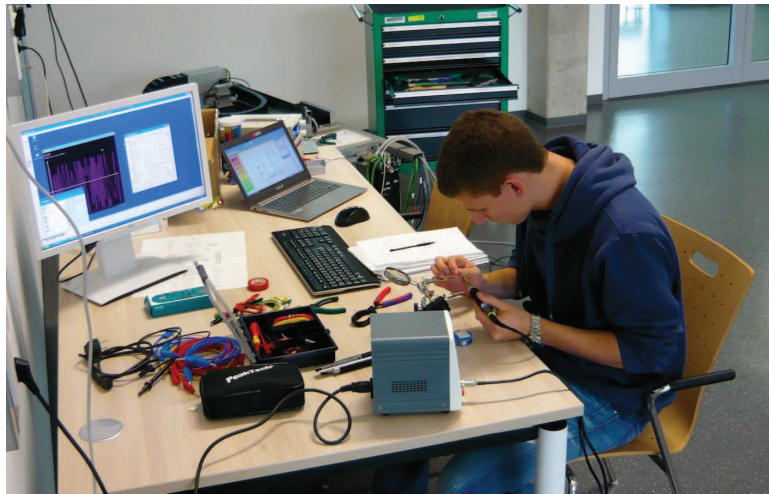


Figure 1: Student S. Scheiterer working on the swing up of an inverted pendulum.

The LTD started to setup a dynamics laboratory. It is equipped with basic devices like an oscilloscope, a multimeter, a soldering station, a workstation with tools, lab power supplies, a dSpace real time machine, different Arduino boards and various accessories. The first challenge is to offer a new dynamics lab tutorial for students covering topics like modelling, simulation, measurement of dynamics and optimal control problems. Some of the experiments are already in preparation like a two degrees of freedom robot used to swing up and control an inverted pendulum (see Figure 1).

The design of another six degrees of freedom robot is based on that of a common industrial jointed-arm robot complemented with a gripper (see Figure 2). This robot is actuated with Dynamixel servos which offer a good compromise between standard model servos and industrial scaled drives. The robot arm will be used to investigate the practical application of optimal control theory, where trajectories optimise certain criteria like energy efficiency or speed. Manufacturing of the accessories starts in the beginning of 2014.

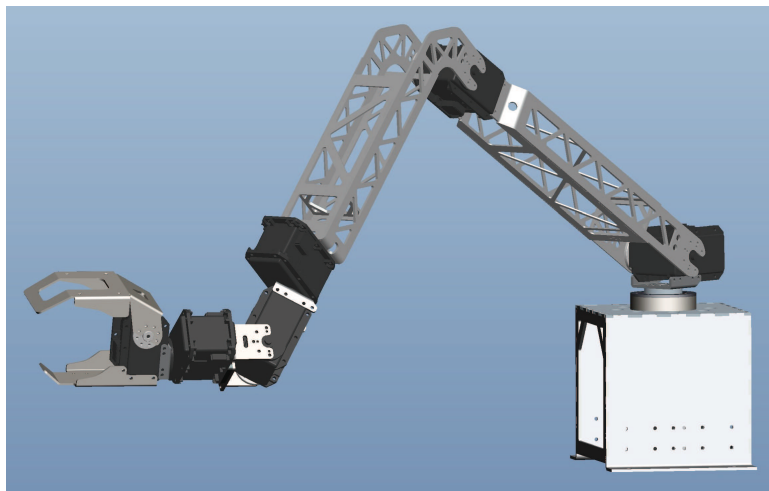


Figure 2: Planned six degrees of freedom jointed-arm robot

#### 4.4 Summer schools



##### **Differential-geometric methods in computational multibody system dynamics**

(16 - 20 September 2013)

Maik Ringkamp and Tobias Gail participated in this CISM course in Udine, Italy. The course was organised by Zdravko Terze and Andreas Müller and held at the lecture room at CISM. Zdravko Terze, Andreas Müller, Olivier Brüls, Carlo Bottasso and Xilun Ding gave lectures on time integration on Lie groups and its application to multibody system dynamics. Furthermore, Todd Murphey talked about variational integrators in optimal control. The CISM was providing us with Italian lunch every day where we could get in contact with the other participants.

##### **Structure-preserving integrators in nonlinear structural dynamics and flexible multibody dynamics**

(07 - 11 October 2013)

This CISM course in Udine, Italy was attended by Odyseas Kosmas, Thomas Leitz and Tobias Gail. The program was organised by Peter Betsch and lectures were given by Peter Betsch, Adrian Lew, Martin Arnold, Alberto Cardona, Johannes Gerstmayr and Ignacio Romero on the topic of higher order and structure preserving integrators. Again the CISM provided great hospitality.

##### **Optimal control, stochastic and mixed Integer programming in energy management**

(14 - 17 October 2013)

Maik Ringkamp participated in the ISAM – TopMath Autumn School at the TU Munich, Germany. The program was organised by Peter Gritzmann, Anusch Taraz and Michael Ulbrich with lectures by Günter Leugering, Alexander Martin and Rüdiger Schultz. Günter Leugering gave lectures on optimal control of energy networks, Alexander Martin talked about piecewise linear functions in energy optimization and Rüdiger Schultz about optimal control, stochastic and mixed integer programming in energy management.

## 5 Publications

### 5.1 Book chapters

1. S. Leyendecker, D. Pekarek, and J.E. Marsden. *Structure preserving optimal control of three-dimensional compass gait*. Modeling, Simulation and Optimization of Bipedal Walking, K. Mombaur, K. Berns (eds.), Vol. 18, pp. 99-116, Springer, 2013.
2. S. Leyendecker, and S. Ober-Blöbaum. *A variational approach to multirate integration for constrained systems*. Multibody Dynamics, Computational Methods in Applied Sciences, J.C. Samin, P. Fiset (eds.), Vol. 28, pp. 97-121, Springer, 2013.

### 5.2 Reviewed journal publications

1. M.W. Koch, and S. Leyendecker. *Structure preserving simulation of monopedal jumping*. Archive of Mechanical Engineering, DOI 10.2478/meceng-2013-0008, Vol. LX, pp. 127-146, 2013.
2. R. Maas, and S. Leyendecker. *Biomechanical optimal control of human arm motion*. Journal of Multi-body Dynamics, DOI 10.1177/1464419313488363, 2013.
3. J. Linn, H. Lang, and A. Tuganov. *Geometrically exact Cosserat rods with Kelvin-Voigt type viscous damping*. Mechanical Sciences, Vol. 4, pp. 79-96, 2013.

### 5.3 Reviewed proceeding publications

1. S. Reitelshöfer, M. Landgraf, J. Franke, and S. Leyendecker. *Qualification of dielectric elastomer actuators as artificial muscles for highly dynamical N-DOF robot kinematics*. In Proceedings of the 6th International Symposium on Adaptive Motion of Animals and Machines, 2 pages, Darmstadt, Germany, 25-26 June 2013.
2. F. Demoures, F. Gay-Balmaz, T. Leitz, S. Leyendecker, S. Ober-Blöbaum, and T.S. Ratiu. *Asynchronous variational Lie group integration for geometrically exact beam dynamics*. In Proceedings of the ECCOMAS Thematic Conference on Multibody Dynamics, DVD, Zagreb, Croatia, 1-4 July 2013.
3. T. Gail, S. Leyendecker, and S. Ober-Blöbaum. *Computing time investigations of variational multi rate integrators*. In Proceedings of the ECCOMAS Thematic Conference on Multibody Dynamics, DVD, Zagreb, Croatia, 1-4 July 2013.
4. M.W. Koch, and S. Leyendecker. *Optimal control of monopedal jumping movements*. In Proceedings of the ECCOMAS Thematic Conference on Multibody Dynamics, DVD, Zagreb, Croatia, 1-4 July 2013.
5. H. Lang, S. Leyendecker, and J. Linn *Numerical experiments for viscoelastic Cosserat rods with Kelvin-Voigt damping*. In Proceedings of the ECCOMAS Thematic Conference on Multibody Dynamics, DVD, Zagreb, Croatia, 1-4 July 2013.
6. R. Maas, and S. Leyendecker. *Muscle paths in biomechanical multibody simulations*. In Proceedings of the ECCOMAS Thematic Conference on Multibody Dynamics, DVD, Zagreb, Croatia, 1-4 July 2013.
7. M. Ringkamp, S. Ober-Blöbaum, and S. Leyendecker. *A numerical approach to multiobjective optimal control of multibody dynamics*. In Proceedings of the ECCOMAS Thematic Conference on Multibody Dynamics, DVD, Zagreb, Croatia, 1-4 July 2013.

## 5.4 Talks

1. F. Demoures, F. Gay-Balmaz, T. Leitz, S. Leyendecker, S. Ober-Blöbaum, and T.S. Ratiu. *Asynchronous variational Lie group integration for geometrically exact beam dynamics*. GAMM Annual Meeting, Novi Sad, Serbia, 18-22 March 2013.
2. T. Gail, S. Leyendecker, and S. Ober-Blöbaum. *Computing time investigations for variational multirate schemes*. GAMM Annual Meeting, Novi Sad, Serbia, 18-22 March 2013.
3. M.W. Koch, and S. Leyendecker. *Optimal control of monopedal jumping movements*. GAMM Annual Meeting, Novi Sad, Serbia, 18-22 March 2013.
4. O.T. Kosmas, and S. Leyendecker. *On frequency estimations in phase fitted variational integrators*. GAMM Annual Meeting, Novi Sad, Serbia, 18-22 March 2013.
5. R. Maas, and S. Leyendecker. *Dynamics of muscle paths in biomechanical simulations*. GAMM Annual Meeting, Novi Sad, Serbia, 18-22 March 2013.
6. M. Ringkamp, S. Leyendecker, and S. Ober-Blöbaum. *Multiobjective optimal control of a four body kinematic chain*. GAMM Annual Meeting, Novi Sad, Serbia, 18-22 March 2013.
7. S. Reitelshöfer, M. Landgraf, T. Schögl, J. Franke, and S. Leyendecker. *Qualifying dielectric elastomer actuators for usage in complex and compliant robot kinematics*. Poster, International conference on Electromechanically Active Polymer (EAP) transducers & artificial muscles, Dübendorf, Switzerland, 25-26 June 2013.
8. F. Demoures, F. Gay-Balmaz, T. Leitz, S. Leyendecker, S. Ober-Blöbaum, and T.S. Ratiu. *Asynchronous variational Lie group integration for geometrically exact beam dynamics*. ECCOMAS Thematic Conference on Multibody Dynamics, Zagreb, Croatia, 1-4 July 2013.
9. T. Gail, S. Leyendecker, and S. Ober-Blöbaum. *Computing time investigations of variational multi rate integrators*. ECCOMAS Thematic Conference on Multibody Dynamics, Zagreb, Croatia, 1-4 July 2013.
10. M.W. Koch, and S. Leyendecker. *Optimal control of monopedal jumping movements*. ECCOMAS Thematic Conference on Multibody Dynamics, Zagreb, Croatia, 1-4 July 2013.
11. H. Lang, S. Leyendecker, and J. Linn. *Numerical experiments for viscoelastic Cosserat rods with Kelvin-Voigt damping*. ECCOMAS Thematic Conference on Multibody Dynamics, Zagreb, Croatia, 1-4 July 2013.
12. R. Maas, and S. Leyendecker. *Muscle paths in biomechanical multibody simulations*. ECCOMAS Thematic Conference on Multibody Dynamics, Zagreb, Croatia, 1-4 July 2013.
13. M. Ringkamp, S. Ober-Blöbaum, and S. Leyendecker. *A numerical approach to multiobjective optimal control of multibody dynamics*. ECCOMAS Thematic Conference on Multibody Dynamics, Zagreb, Croatia, 1-4 July 2013.
14. I.S. Kardaras, and O.T. Kosmas. *Using simulated annealing algorithms to solve the Schroedinger equation in muonic atoms*. International Conference on Mathematical Modeling in Physical Sciences, Prague, Czech Republic, 1-5 September, 2013.
15. O.T. Kosmas, and D.S. Vlachos. *Energy fitted discrete Lagrangian integrators*. International Conference on Mathematical Modeling in Physical Sciences, Prague, Czech Republic, 1-5 September, 2013.

16. O.T. Kosmas, and D. Papadopoulos. *Multi-symplectic structure of numerical methods derived using nonstandard finite difference schemes*. International Conference on Mathematical Modeling in Physical Sciences, Prague, Czech Republic, 1-5 September, 2013.
17. S. Leyendecker, S. Ober-Blöbaum, and T. Gail. *Structure preserving integration of constrained multirate systems*. International Conference on Scientific Computation and Differential Equations (SciCADE), Valladolid, Spain, 16-20 September 2013.
18. M.W. Koch, and S. Leyendecker. *Optimal control of monopedal jumping movements*. 5-th GACM Colloquium on Computational Mechanics, Hamburg, Germany, 30 September - 02 October 2013.
19. M.W. Koch, and S. Leyendecker. *Structure preserving simulation of non-smooth dynamics and optimal control*. Bayerisch Tirolerisches Mechanik Kolloquium, Erlangen, Germany, 23 November 2013.
20. S. Leyendecker. *BIOSOL, Ohm-Krabbler und künstliche Muskeln*. (Bionicum Forschung) Statusseminar Bionik in Bayern, Nuremberg, Germany, 28 November 2013.
21. S. Leyendecker. *A discrete variational approach to optimal control problems in multibody dynamics*. Invited lecture, Eleonore-Treffitz-Vorlesung, TU Dresden, Dresden, Germany, 18 December 2013.

## 6 Social events

### Berg 2013



### New building



### Nikolaus hike



### Christmas party 2013 together with LTM

